Computers and Geotechnics 41 (2012) 36–56

Contents lists available at SciVerse ScienceDirect

Computers and Geotechnics

journal homepage: www.elsevier.com/locate/compgeo

Effect of hydraulic hysteresis on seepage analysis for unsaturated soils

Chao Yang [a,*], Daichao Sheng [a,1], John P. Carter [b,2]

[a] Centre for Geotechnical and Materials Modelling, The University of Newcastle, NSW 2308, Australia
[b] Faculty of Engineering and Built Environment, The University of Newcastle, NSW 2308, Australia

ARTICLE INFO

Article history:
Received 24 July 2011
Received in revised form 21 September 2011
Accepted 22 November 2011

Keywords:
Soil water characteristic curve
Hydraulic hysteresis
Unsaturated soils
Soil cover

ABSTRACT

This paper describes a study into the effects of hysteresis on the hydraulic behaviour of unsaturated soil covers. The Richards equation is coupled with the hysteretic soil water characteristic curves (SWCCs), to describe water flow in unsaturated soils. A linear scanning curve on semi-logarithmic scales is used to describe the hydraulic behaviour within the main hysteretic loop in unsaturated seepage problems. The proposed approach is implemented for one-dimensional flow problems using the finite difference method. A comparison of predictions of the proposed hysteretic model with those of the traditional non-hysteretic model is carried out first. For the assumed scenario of a compacted clay cover, the non-hysteretic model using the main drying SWCC leads to significantly different results than the hysteretic model, further demonstrating the necessity of accounting for hysteresis in unsaturated seepage analysis. Moreover, three infiltration tests on layered soil columns are simulated with the proposed hysteretic model. Results show that hysteresis plays an important role in the seepage analysis of unsaturated soils subjected to cyclic drying and wetting. The hysteretic model is suggested for use in the design and evaluation of the hydraulic performance of soil covers.

1. Introduction

Various types of soil cover systems such as compacted covers (e.g., [31,3]), capillary covers (e.g., [41,45,24,5,6]), geosynthetic clay liner covers [29,30], and multilayer soil covers (e.g., [52,37,44]), have been implemented in projects involving landfills and mining tailings disposal to minimise their potential risk to surrounding environments. In the last two decades or so many laboratory experimental studies (e.g., [53]), field monitoring (e.g., [32]) and numerical modelling studies (e.g., [38,34,33,14]) have been conducted on the performance of soil covers. However, due to the diversity of variables like soil types, climatic issues, plant species and topographic features, the design of effective and economic soil covers still remains a great challenge. Among the complicated boundary conditions that will be considered, cyclic wetting and drying induced by precipitation and evapotranspiration is one of the most common exterior actions on the soil covers. This paper is dedicated to studying the hysteretic effects of the soil water characteristic curves (SWCCs) on the hydraulic behaviour of soil covers subjected to cyclic climatic drying and wetting processes.

To assess the hysteretic hydraulic behaviour of soil covers, the *h*-based Richards equation [39,8,15] is employed, which requires knowledge of both the SWCC function (the soil water potential, ψ, and the volumetric water content, θ) and the hydraulic conductivity function (the hydraulic conductivity, k versus θ or ψ). Meanwhile, hydraulic hysteresis, known to be characteristic in SWCCs of unsaturated soils, generally refers to the non-unique relationship between the soil water potential and the water content, whereby considerable variation in the water content can occur under the same soil water potential depending on the preceding sequence of drying and wetting [19]. In the literature, hydraulic hysteresis is usually described by the main drying–wetting bounding curves and the interior scanning curves.

The main drying–wetting bounding curves are usually constructed using SWCC equations such as those widely used in the literature (e.g., [48,16]). On the other hand, the interior scanning curves are usually scaled from the main drying–wetting loop with various kinds of scaling approaches, for instance, the point method [12], the slope method [23], the linear method [20], the domain method [36] and the bounding surface method [27]. The differences in those different scanning models are not always significant in practical applications. Jaynes [23] compared the first four methods listed above and concluded that all these four methods have the same degree of accuracy in simulating scanning curves in wetting–drying cycles in soils. However, due to the implementation complexity or possible numerical problems (such as the false pumping effects and convergence problems) associated with these

* Corresponding author. Tel.: +61 2 49215893; fax: +61 2 49216991.
E-mail addresses: chao.yang@newcastle.edu.au (C. Yang), daichao.sheng@newcastle.edu.au (D. Sheng), john.carter@newcastle.edu.au (J.P. Carter).
[1] Tel.: +61 2 49215746; fax: +61 2 49216991.
[2] Tel.: +61 2 49216025; fax: +61 2 49217062.

0266-352X/$ - see front matter © 2011 Elsevier Ltd. All rights reserved.
doi:10.1016/j.compgeo.2011.11.006

methods, the linear method on the semi-logarithmic scales, will be used to scan the hysteretic $\psi - \theta$ relation within the main drying–wetting loop. This scanning method is found to be simple to use, requires relatively little data storage, and still provides reasonable accuracy.

The hydraulic conductivity of an unsaturated soil is more challenging to quantify, as it can span over multiple orders of magnitude [13]. It is commonly believed that the pore-size distribution determines the distribution of pore water in the soil matrix at a given soil water potential. Meanwhile, as the water only flows through the water phase in the porous medium, the dependency of water flow on the pore water distribution becomes apparent. In other words, with a constant pore-size distribution, a unique relationship between the hydraulic conductivity and the water content should be maintained [28]. This unique relationship has also been validated by Fredlund et al. [17] for Guelph loam and Meerdink et al. [31] for Wenatchee silty clay.

Similar to SWCCs, various hydraulic conductivity functions for unsaturated soils have been proposed, either based on empirical curve fitting or statistical methods. In the empirical methods, the hydraulic conductivity is usually expressed as a closed-form function of matric suction [4,18] or water content [2,7]. By contrast, the statistical methods are primarily based on the fact that both the hydraulic conductivity and the SWCCs are determined by the pore-size distribution and the characteristic drying and wetting water radii distribution [9,35]. Even though the statistical models probably have the highest accuracy in predicting scanning curves for different porous media, they are more difficult to use in calculation and design. At the same time, empirical hydraulic conductivity functions in terms of suction are not unique due to hydraulic hysteresis. However, as stated by Fredlund and Rahadjo [15], the hydraulic conductivity shows essentially no hysteresis when cross-plotted against the volumetric water content. Moreover, this uniqueness between the hydraulic conductivity in unsaturated soils and the water content further simplifies the numerical implementation of the seepage analysis. Thus the hydraulic conductivity will be defined in terms of the volumetric water content in this paper.

Besides the theoretical research mentioned above, a large number of laboratory and on-site experiments have been carried out to study the hydraulic behaviour of unsaturated soil covers. Meerdink et al. [31] investigated the hydraulic conductivity of compacted Wenatchee silty clay and found a significant hysteretic relationship between the hydraulic conductivity and suction. Stormont and Anderson [46], Yang et al. [54], and Indrawan et al. [22] used the infiltration column apparatus to study the transient hydraulic behaviour of two-layer soil columns, whereas Tami et al. [47] conducted infiltration column tests to study the steady-state behaviour of unsaturated slopes. These experiments all confirmed that hydraulic hysteresis can affect the seepage in unsaturated soils.

For unsaturated soil covers, there have been very few numerical studies that take into account the effects of hydraulic hysteresis on seepage. Tami et al. [47] and Indrawan et al. [22] modelled their own experiments. Yanful et al. [51] numerically assessed the influence of several cover properties and the hydrogeological parameters on the cover performance. Adu-wusu et al. [1] also simulated the field performance of two soil covers. In all these analyses, hydraulic hysteresis was either ignored or was manually added to the software so that the drying or wetting processes occur simultaneously over the entire soil domain. However, all these authors pointed out that hysteretic effects can significantly affect the accuracy of numerical simulation of soil covers, and suggested that hydraulic hysteresis should be considered in assessing soil cover performance.

Because it is seldom true that the entire soil domain simultaneously experiences drying or wetting in a synchronised manner, it is usually not sufficient merely to adjust the soil water relationship according to the boundary conditions. Imposing a sudden change in the relationship between the soil water potential and water content (and hydraulic conductivity) may also lead to convergence problems when solving the seepage equation. In reality, it is common that some parts of the soil domain will experience drying whereas other parts will simultaneously experience wetting. In other words, the change of drying and wetting conditions at a given point in the soil is part of the solution of the seepage equation and may not be synchronous with the boundary conditions. Therefore, a more realistic and robust method to solve this problem is to integrate hydraulic hysteresis into the seepage equation and treat it as a type of material non-linearity.

A study of the effect of hydraulic hysteresis on seepage in unsaturated soils is carried out in this paper. The hysteretic soil water characteristic curve equation is incorporated into Richards' equation for seepage in unsaturated soils. Comparisons between the proposed hysteretic model (HM) and the traditionally non-hysteretic model (NHM) are then carried out on soils with significant hysteresis (i.e., compacted clay covers). The performance of the HM is further compared with three experimental infiltration tests on two-layer capillary soil columns to demonstrate the validity of the approach.

2. Formulation

2.1. Richards' equation

In this paper, the h-based Richards equation [8,15] is used to evaluate the seepage in unsaturated soils. For simplicity, the vapour conductivity is not considered here, and thus the Richards equation in one-dimensional space can be expressed as follows:

$$\frac{\partial}{\partial y}\left[k_y \cdot \frac{\partial h}{\partial y}\right] = \gamma_w \cdot m_2^w \cdot \frac{dh}{dt} \tag{1}$$

where k_y is the hydraulic conductivity in the vertical direction, y; m_2^w is the coefficient of water storage consistent with the slope of the SWCCs; and h is the total hydraulic head, defined as the sum of the capillary pressure head and the elevation head. γ_w is the unit weight of water. Note that constant soil volume is assumed in the seepage analysis presented in this paper.

Considering the intrinsic correlation between the hydraulic conductivity and the pore-size distribution and the assumption that the volume change along drying or wetting paths is negligible, it is preferable to formulate the hydraulic conductivity in terms of the normalised volumetric water content. Averjanov [2] proposed such an equation and this equation is slightly modified here:

$$k_r(\theta) = c_k \cdot (\Theta)^{\lambda_k} \tag{2}$$

where $k_r(\theta)$ is the normalised hydraulic conductivity, $k_r(\theta) = \frac{k(\theta)}{k_s}$, with $k(\theta)$ and k_s being the hydraulic conductivities in unsaturated and saturated states, respectively; λ_k is an empirical constant highly dependent on the pore size distribution or soil porosity alternatively; and c_k is a correction coefficient introduced in this paper which can be determined from experimental data. It has been found that λ_k tends to increase with increasing soil density [40] and has quite a wide range of values from 2.57 to 52.12 [26,40]. In this paper, an initial value of 3.5 proposed by Averjanov [2] is first adopted in the comparative studies between the hysteretic model and the non-hysteretic model, but the value of λ_k is then adjusted in the validation analyses according to the specific soils involved.

Parameter Θ is the normalised volumetric water content and is written as follows:

$$\Theta = \frac{\theta(\psi) - \theta_r}{\theta_s - \theta_r} \tag{3}$$

where $\theta(\psi)$ is the volumetric water content which is a function of the soil water potential (ψ); θ_s and θ_r are the saturated and residual

volumetric water contents, respectively. Chiu and Shackelford [10] suggested that the maximum volumetric water content after steady-state flow, θ_m, should be used instead of θ_s, but this suggestion is not considered any further in this work.

The normalised volumetric water content can also be expressed in terms of degree of saturation:

$$\Theta = \frac{S_r(\psi) - S_{res}}{1 - S_{res}} = S_e \tag{4}$$

where S_{res} is the relative residual degree of saturation, and S_e is also called the normalised or effective degree of saturation. From the above equation, it can be seen that the normalised volumetric water content is equivalent to the effective degree of saturation when the volume remains constant during seepage.

2.2. Soil water characteristic curve (SWCC)

Dye et al. [13] found that the uncertainty associated with the choice of SWCC models is insignificant and within the range of expected empirical data scatter. In this study, the van Genuchten [48] equation is used for convenience:

$$\Theta = S_e = \left(\frac{1}{1 + (\alpha\psi)^n}\right)^m \tag{5}$$

where α, n, m are fitting parameters. In order to keep the model simple, m can be obtained according to van Genuchten [48]:

$$m = 1 - \frac{1}{n} \tag{6}$$

In more general cases where there is enough information about the soil water characteristic behaviour, it is better to leave the parameters n and m as independent quantities, as pointed out by Fredlund and Xing [16]. Besides, α^{-1} is usually considered to be related to the so-called air entry potential value for low ratios of m/n, while for high values of m/n it is roughly equal to the potential at the inflection point of the soil water characteristic curve [49]. This observation will help in the determination of parameters in the future modelling.

Parameters n, m, θ_r and θ_s are assumed to be the same for both the main drying and main wetting curves. The parameter α is related to the air entry value and is used to differentiate the main drying curve from the main wetting curve. Following the proposal of Kool and Parker [25], the hysteretic ratio, ξ, defined as:

$$\xi = \frac{\alpha_w}{\alpha_d} \tag{7}$$

is adopted as an indication of the degree of hydraulic hysteresis in an unsaturated soil.

2.3. Scanning curves

Considering the simplicity and efficiency of linear scanning curves, the following incremental expression is adopted:

$$\frac{dS_r}{d(\log\psi)} = -\kappa \tag{8}$$

where κ_s is the slope of the scanning curve in semi-logarithmic coordinates.

However, it should be noted that the scanning curve may not intersect with the expected main drying or wetting curve, especially near fully saturated and extremely dry conditions. Fig. 1 shows such a case where the slope of the scanning curve (κ_{s0} at Point A) is relatively large and as such leads to the wrong intersection with the main curve (Point B). In order to ensure a proper scanning within the main drying and wetting curves, the slope of the scanning curve should be restrained. In this study, the following constraint is imposed on the slope of the scanning curves:

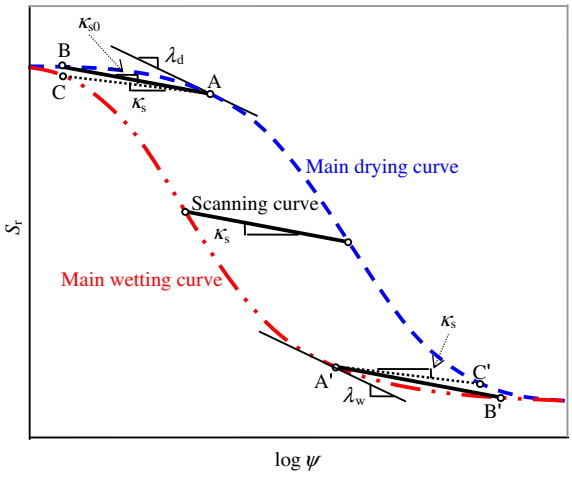

Fig. 1. Constraints on the evolution of the slope of the scanning curve, κ_s.

$$\kappa_s = r_{\kappa s}\kappa_{s0} < r_{\kappa s}\lambda_{w/d} \tag{9}$$

where κ_{s0} is an initial user-defined value of κ_s in the scanning process, $\lambda_{w/d}$ is the slope of the main wetting or drying curve at the transition point between wetting and drying, and $r_{\kappa s}$ is a positive constant between 0 and 1, and the subscripts w, d and s represent the wetting, drying and scanning processes, respectively.

With the above constraint, a more reasonable scanning curve starting from A can be constructed (Fig. 1), which results in a proper intersection with the main wetting curve at C. The same approach can also be used to deal with extremely dry conditions (A′ in Fig. 1). The slope of the main drying and wetting curves ($\lambda_{w/d}$) is usually a function of soil water potential (Fig. 2), which is important to determine the proper values of both κ_{s0} and $r_{\kappa s}$. Iteration may be required to achieve proper and accurate values for κ_{s0} and $r_{\kappa s}$.

The soil water characteristic model mentioned above is assumed to be independent of the volumetric change during the cyclic drying and wetting processes. This is a coarse assumption. However, as this paper is only concerned with seepage in unsaturated soils, the dependency of SWCCs on stress and deformation is less significant here. A coupled formulation that incorporates mechanical and hydraulic behaviour of unsaturated soils may be required if the voids ratio of the soil changes significantly [42,43].

2.4. Definition of matric suction

In order to maintain accuracy, stability and convergence of the numerical solution of Richards' equation near fully saturated and

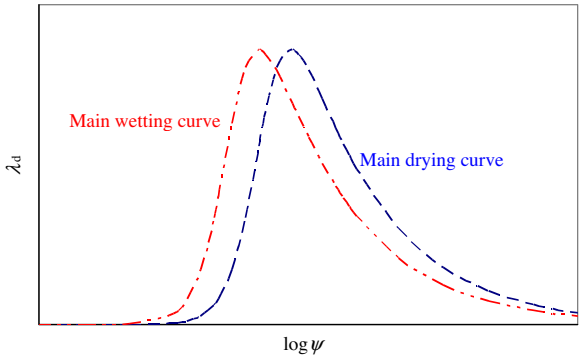

Fig. 2. Values of the slopes of two main SWCCs against the suction.

extremely dry states, the matric suction is assumed to be equivalent to the soil water potential. By assuming the pore air is connected to the atmosphere in engineered soil covers, the matric suction is defined as the negative pore water pressure, and expressed as:

$$\psi = \begin{cases} -p_{w0}, & p_w \geq p_{w0} \\ -p_w, & p_{wmin} \geq p_w < p_{w0} \\ -p_{wmin}, & p_w > p_{wmin} \end{cases} \quad (10)$$

where p_{w0} is denoted as the maximum negative pore water pressure, which can take a value between −1 kPa and −0.1 kPa [50], p_{wmin} is the minimum negative pore water pressure when the water content is below the residual value [11]. In this paper, p_{w0} and p_{wmin} are given values of −0.001 and −999,999 kPa, respectively.

3. Finite difference model

The finite difference method is used to solve the seepage equation that incorporates the hysteretic soil water behaviour. A backward time stepping scheme is used to solve the non-linear discretised system of equations. Only one-dimensional seepage is considered in this paper. The soil column is either uniform or has a layered soil profile. The uniform soil column has a height of 1.50 m, an initial mesh spacing of 0.10 m and a time step of 0.001 days, and is used in the comparative study of seepage with and without hydraulic hysteresis.

3.1. Boundary and initial conditions

The Neumann boundary condition is employed to simulate precipitation and evaporation at the top surface of the soil column. For simplicity, the precipitation and evaporation are considered as a prescribed water flux into and out of the soil column, thereby inducing cyclic wetting and drying processes in the soil. Once the top surface soil is fully saturated, a run-off mechanism is activated so that the boundary flux stops until the soil becomes unsaturated again. To simulate a well-functioning soil cover, an impermeable boundary condition is applied at the bottom surface of the soil column. It is worth noting that although there is no flux across the bottom boundary, internal readjustment of the moisture content in the cover, including at the bottom boundary, is entirely possible. This will be illustrated in the next section. In addition, no horizontal flow is considered here.

An initial matric suction (ψ_0 = 600 kPa) is assumed throughout the soil column, and the hydraulic heads in the soil can be obtained correspondingly. A cyclic drying–wetting process with an equal absolute flux of 10 mm/day is imposed on the top surface of the soil column. Each drying or wetting lasts for a period of 2 days, and a series of such cyclic actions are simulated. Because of the abrupt change of the top boundary condition between any two adjacent drying and wetting events, a smaller time step (0.0001 days) is used to ensure the convergence of the simulation. The values of various parameters used in the numerical analysis are listed in Table 1.

3.2. Hydraulic state in hysteretic loop

To control the hydraulic path transferring between the main SWCC loop and the scanning curve, the method depicted in Fig. 3 is introduced, together with the change of hydraulic head (Δh). With the starting point known, the scanning curve can be located according to Eq. (8), for instance, the wetting scanning curve A–A′ in Fig. 3. During the wetting process ($\Delta h > 0$), the degrees of saturation (S_{rB_d}, S_{rB_w}, and S_{rB_s}) on these three curves, namely the main drying, main wetting and scanning curves, can be obtained for any given suction. Consequently, for the wetting path A–B–C–D, the following criterion can be used to determine the hydraulic state:

$$S_r = \begin{cases} S_{rB}, & S_{rB_w} < S_{rB} < S_{rB_d} \quad \text{(Wetting scanning)} \\ S_{rC}, & S_{rC_s} < S_{rC} < S_{rC_d} \quad \text{(Main wetting)} \end{cases} \quad (11)$$

Similarly, for the drying process ($\Delta h < 0$) D–E–F in Fig. 3, the corresponding criterion is:

$$S_r = \begin{cases} S_{rE}, & S_{rE_w} < S_{rE} < S_{rE_d} \quad \text{(Drying scanning)} \\ S_{rF}, & S_{rF_d} < S_{rF} < S_{rF_s} \quad \text{(Main drying)} \end{cases} \quad (12)$$

It should be noted that the scanning curve is updated according to the starting point, such as A or D. Due to space limit, more detailed description about the hydraulic state transition and other specific numerical techniques employed can be referred to Yang et al. [55].

Table 1
Values of parameters for the conceptual scenario.

	Symbol	Unit	Assumed clay
Saturated volumetric water content	θ_s	–	0.380
Residual volumetric water content	θ_r	–	3.800×10^{-3}
Hydraulic conductivity			
Saturated hydraulic conductivity	k_s	m/d	8.640×10^{-4}
Parameters	c_k	–	1.000
	λ_k	–	3.500
Drying curve			
Fitting parameters	α_d	kPa^{-1}	0.010
	n_d	–	1.226
Wetting curve			
Fitting parameters	α_w	kPa^{-1}	0.014
	n_w	–	1.226
Scanning curve			
Scanning slope	κ_s	kPa^{-1}	4.600×10^{-2}
	$r_{\kappa s}$	–	0.200

4. Modelling results and discussion

The proposed hysteretic model, HM, is first compared with the traditional non-hysteretic model, NHM, which employs only one drying (or wetting) SWCC. The hysteretic model is further compared with experimental data.

4.1. Comparison between HM and NHM

The assumed scenario is a compacted clay cover, with high air entry value (α_d = 0.01). The comparative study is mainly focused on three major properties, namely, the suction, the degree of saturation and the hydraulic conductivity. The flux velocity and the change of water storage are also taken into account to help understand the mechanism behind the complex hydraulic behaviour of unsaturated soils.

The hydraulic paths (the relationship between the degree of saturation and the suction) at different elevations of the soil column studied are shown in Fig. 4. At the top surface (y = 1.5 m), the HM and NHM exhibit totally different hydraulic paths (Fig. 4a), though subjected to the same exterior actions. It can be seen that the suction predicted by the HM covers a wider range of values than that by the NHM. This is considered to be attributable to the scanning process in the HM, which produces a rapid change in suction with respect to the water content. As shown in Fig. 4a, upon the first drying process in the HM, the hydraulic state initially at Point A moves along the main drying curve to Point B. In the subsequent wetting, the hydraulic state at y = 1.5 m departs from the main drying curve (Point B),

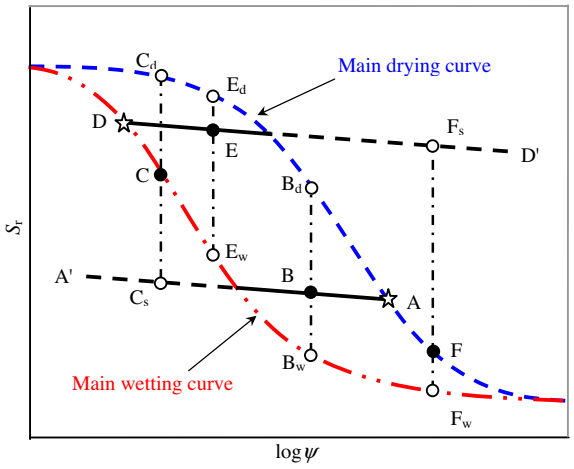

Fig. 3. Determination of hydraulic state in hysteretic SWCC loops.

moves along the scanning curve (B–C), and then reaches the main wetting curve (Point C), and finally moves along the main wetting curve to Point D. In the next drying cycle, the hydraulic state starts from the main wetting curve (Point D), traverses the scanning zone (D–E), and then follows the main drying curve to Point F. Similar hydraulic paths are predicted by the HM in the following wetting (F–G–H, J–K–L) and drying (H–I–J, L–M–N) processes. Similar conclusions can also be achieved at other elevations of the soil column, e.g., y = 0.5, 0.0 m (Fig. 4b and c). In addition, it is worth noting that at the bottom surface of the soil column (y = 0.0 m), the hydraulic path does not make an enclosed loop after the series of cyclic drying–wetting (Fig. 4c). On the other hand, the NHM only simulates the hydraulic paths along the main drying curve, and leads to smaller variations in suction but larger variations in water content, which becomes more obvious with increasing depth. This difference is attributed to the inclusion of hysteresis in the seepage analysis of unsaturated soils.

Results of the hydraulic conductivity at y = 1.5 m predicted by both the HM and NHM are given in Fig. 5. From the combination of the prescribed hydraulic conductivity function (Eq. (2)) and the adopted SWCC (Eq. (5)), the variation of hydraulic conductivity with matric suction can be deduced. As shown in Fig. 5, the development of hydraulic conductivity under the cyclic drying and wetting processes resembles the hydraulic paths discussed above.

However, with only the hydraulic paths obtained above it would be difficult to track the hydraulic state in an unsaturated soil subjected to different initial and boundary conditions. Therefore, the evolution with time of suction and degree of saturation is presented in Figs. 6 and 7, respectively. It can be observed that the HM predicts a relatively larger variation in suction (Fig. 6), but a more gradual variation in degree of saturation (Fig. 7), when compared with the NHM under the same initial and boundary conditions. This difference between the HM and NHM becomes more significant with increasing depth, which is further corroborated in Fig. 8. In addition, the transition points between the main SWCC loop and the scanning curve can be clearly observed in Figs. 6 and 7, which are denoted by the dashed encircled points.

The response delay in depth with respect to the imposed top boundary condition (y = 1.5 m) is presented in Fig. 8 for the first drying cycle. The response delay predicted by both the HM and NHM increases with depth, consistent with the travelling time of water to the target elevation. The HM predicts a much shorter response delay than the NHM, and the difference increases rapidly with depth, consistent with the conclusion obtained above (Fig. 4). In other words, soils with more apparent hydraulic hysteresis are more sensitive to exterior actions. On the other hand, it can be concluded that the HM is liable to predict a higher average flux velocity than the NHM. This conclusion is further verified in Fig. 9, by comparing the flux velocities at the bottom surface of the soil column predicted by the HM and NHM, both of which respond synchronically to the variation of hydraulic state in the upper part of the soil column. Since the NHM tends to predict a lower flux velocity and a longer water infiltration time, caution should be exercised when using the traditional non-hysteretic model to design and evaluate the efficiency of soil covers subjected to frequent drying and wetting cycles.

5. Experimental validation

In the previous section, predictions of the proposed hysteretic model (HM) have been compared with those of the traditional non-hysteretic model (NHM). It was noted that different hydraulic behaviours are predicted by these two models. In this section, the proposed hysteretic approach is validated against the results of laboratory experiments. Due to the difficulty in conducting seepage experiments in compacted clay covers, very limited data is available for this type of soil to validate the proposed hysteretic model (HM). However, seepage experiments in covers composed of sands are not rare, and although the hydraulic hysteresis inherent in these granular materials is not as pronounced as in finer-grained soils, relatively complete information can be collected and employed as a first step to test the validity of the HM model. In the following, three infiltration tests on two-layer capillary soil columns are simulated with the HM.

The capillary cover, usually composed of a fine-over-coarse soil layer sequence, has been proposed as a possible alternative to the compacted soil covers often used for solid waste-disposal systems. Due to the large contrast in hydraulic conductivities between these two layers, the mechanism of capillary tension limits water's downward movement temporarily and further prevents the formation of acid rock drainage in mine tailings. Stormont and Anderson [46] reported that the more uniform and coarse the lower layer is, the more effective the capillary barrier. With in situ experiments, Bussiere et al. [6] further confirmed the capillary barrier effect is capable of maintaining a high degree of saturation in the upper finer layer and thus limiting the migration of oxygen and water into the bottom mining waste layer.

Stormont and Anderson [46], Yang et al. [54], and Indrawan et al. [22] independently carried out laboratory infiltration column tests on unsaturated soils and provided high quality data for validation of numerical analysis. The proposed hysteretic model will be validated against these test data.

Considering the mechanism of capillary barrier covers as indicated by Stormont and Anderson [46], the following hypothesis is incorporated into the proposed hysteretic model. Water breakthrough is controlled by the breakthrough suction of the lower layer, ψ_w. When the suction at the upper side of the capillary interface decreases to or below ψ_w, a continuous network of pore water is established throughout the two-layer soil column. The barrier then fails and water flows into the lower layer. Furthermore, when the infiltration stops or evaporation dominates at the top surface, the initiated breakthrough will cease and the capillary barrier is restored at the capillary interface. Thus, a restoration suction, ψ_d, is defined in the capillary barrier restoration process. However, due to hysteresis in the SWCCs of the coarser layer, the restoration suction is different from the breakthrough suction, and it is generally true that $\psi_d > \psi_w$.

5.1. Case 1: Soil column of silty sand over pea gravel [46]

Stormont and Anderson [46] carried out infiltration tests on soil columns of silty sand over pea gravel (SP), concrete sand over pea

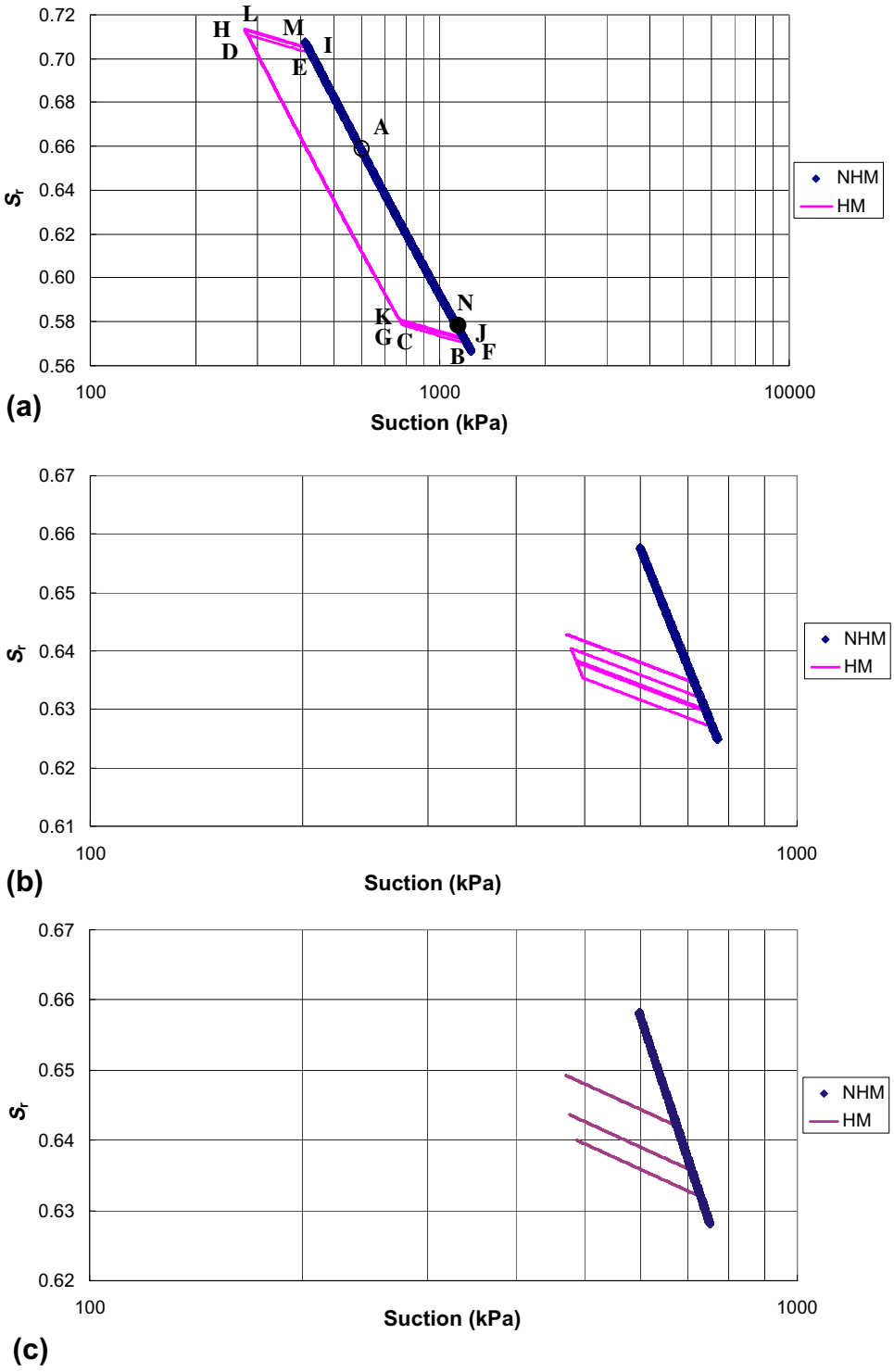

Fig. 4. Hydraulic paths at different elevations of a one-layer soil column subjected to cyclic drying–wetting: (a) $y = 1.5$ m; (b) $y = 0.5$ m and (c) $y = 0.0$ m.

gravel (CP), and silty sand over concrete sand (SC) to investigate the capillary effects of an underlying coarser layer. In this paper, only the silty sand over pea gravel column (SP) is used to validate the proposed hysteretic model. The soil column SP consisted of a 700 mm thick layer of finer silty sand overlying a 100 mm thick coarser pea gravel layer. Suction changes were monitored using tensiometers in the upper silty sand layer. The detailed experimental procedure can be found in Stormont and Anderson [46].

The soil column SP was first left to equalise for 5 days after construction. Rainfall with an intensity of 2.51×10^{-3} m/d was imposed for 21.6 days, and by that time the wetting front had reached the finer–coarser soil interface. A suction of about 7.00 kPa was achieved throughout the upper finer layer. According to the known experimental results, the starting time of the normal rainfall test with the same intensity, designated as D-0 in this paper, was set to the original Day 26.6. The rainfall stopped on D-31 (original Day 57.7), and then the soil column was kept static to allow moisture redistribution until D-40 (original Day 66.6).

The initial condition for the rainfall event was set according to the above experimental results. Accordingly, constant suctions of

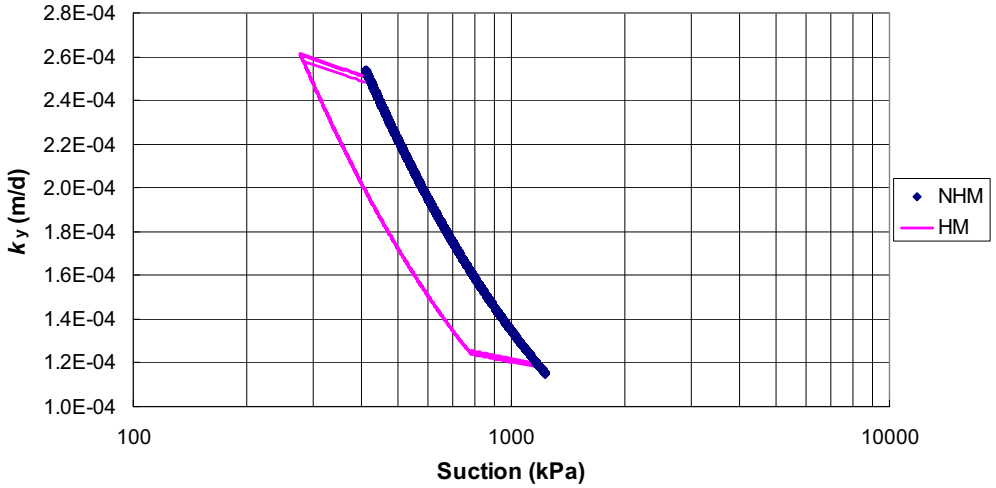

Fig. 5. Variation of the hydraulic conductivity of a one-layer soil column at $y = 1.5$ m.

6.86 kPa and 0.80 kPa were imposed on the upper finer and lower coarser layers, respectively. Both layers were assumed to stay initially on the main wetting curve. As indicated by Stormont and Anderson [46], the breakthrough and restoration heads essentially depend only on the lower coarser layer, not on the infiltration rate and the overlying finer soil properties. For the pea gravel used as the lower coarser layer, Stormont and Anderson [46] observed that the breakthrough suction remained between 0.15 kPa and 0.30 kPa, and the restoration suction between 0.64 kPa and 0.94 kPa. In this simulation, considering the SWCCs for pea gravel, suctions of 0.30 kPa and 0.80 kPa were used in the model as the breakthrough and restoration suctions, respectively. In addition, in order to improve the efficiency and convergence of the numerical analysis, the lower coarser layer was assumed to be 0.30 m thick (instead of its actual thickness of 0.10 m), which makes the total height of the entire soil column analysed to be 1.00 m. The mesh size in both layers was 0.05 m. An initial time step of 0.001 days was used in the numerical analysis. The parameter values used in this simulation are listed in Table 2. The SWCCs for the silty sand and pea gravel are depicted in Fig. 10.

The performance of the hysteretic model in simulating this infiltration test is compared with the experimental results in Figs. 11–13. Fig. 11 shows the profiles of suction, degree of saturation and hydraulic conductivity in the soil column. It indicates that the model simulates the suction development during the infiltration fairly well in the upper silty sand layer (Fig. 11a). At D-7, the discrepancy between the measured and predicted suctions at $y = 0.9$ m might be attributed to the inaccurate description of the initial state. With continuous infiltration, the suctions in the upper layer first decrease, and then increase during the following moisture redistribution process. The non-static hydro-equilibrium during the entire test is well captured, corroborated by a series of suction profiles with unit slope. Meanwhile, the water content increases gradually with infiltration (Fig. 11b). In Fig. 11c, the predicted hydraulic conductivity illustrates similar changes as the degree of saturation. In addition, it should be noted that data for suctions at $y = 1.0$ m are extrapolated from those actually measured in the lower part of the soil column.

The evolution of hydraulic properties at or near the finer–coarser interface can be found in Fig. 12. It can be seen that the suction at the interface ($y = 0.30$ m) decreases continuously (Fig. 12a) when the corresponding water content increases with the infiltration (Fig. 12b). On D-24, the suction at the upper side of the interface decreases below the breakthrough suction, 0.30 kPa. In the meantime, the respective water content approaches saturation (Fig. 12b). Hence, a continuous network of pore water is bridged between the finer and coarser layers and percolation into the lower layer occurs. Upon this percolation, the suction at the lower side of the interface ($y = 0.25$ m) drops abruptly (Fig. 12a). The loss of water from the finer side of the interface leads to a large increase in suction at $y = 0.30$ m. Once the suction at $y = 0.30$ m exceeds the restoration threshold, the assumed capillary mechanism is activated again. So the downward flux ceases at the interface and then the capillary barrier is completely recovered. As time elapses, soils near the interface reach a relatively stable state. Stormont and Anderson [46] observed that the breakthrough lasts for about 10 days in the soil column, which is not well captured by the model. Some numerical oscillation also exists during the breakthrough process. These problems might be attributed to the large contrast in the hydraulic properties between the upper and lower layers combined with the use of a finite difference scheme for solution of the governing differential equation.

To further illustrate the capacity of the proposed hysteretic model, the hydraulic paths experienced by soils at different elevations ($y = 1.00$, 0.65, 0.30 and 0.25 m) are presented in Fig. 13. It is interesting to note that the soil matrix at the top surface ($y = 1.00$ m) experiences an initial drying during the rainfall period, as found in Fig. 13a. Departing from the main wetting curve (Point A), the silty sand at $y = 1.00$ m moves along the scanning curve (A–B) towards and then on the main drying curve (B–C). This can be explained by the net outflow of water from this point, since the infiltration rate (2.51×10^{-3} m/d) is far less than the corresponding hydraulic conductivity of silty sand (3.16×10^{-2} m/d). According to the non-static equilibrium stated by Stormont and Anderson [46], extrapolated data from the measured results at $y = 1.00$ m can corroborate the above analysis (Fig. 11a). Following the first drying at $y = 1.00$ m, the hydraulic conductivity at the top of the soil column decreases and eventually produces a flux balance at this point. Afterwards, the rainfall starts to wet the soil matrix at the top, leading to a hydraulic path first along the scanning curve (C–D) and then along the main wetting curve (D–E). Once the infiltration is stopped, drying at $y = 1.00$ m is reactivated and drives the hydraulic path onto the scanning curve (E–F) again. Clearly, with the known hydraulic path, the behaviour of the unsaturated soil under infiltration can be better understood.

For soil at $y = 0.65$ m (Fig. 13b), a similar hydraulic path to that at $y = 1.00$ m is observed. The only difference is that soil at $y = 0.65$ m never reach the main drying curve, which can be attributed to the quicker achievement of water flow balance from the first drying. For the soil at the upper side of the finer–coarser

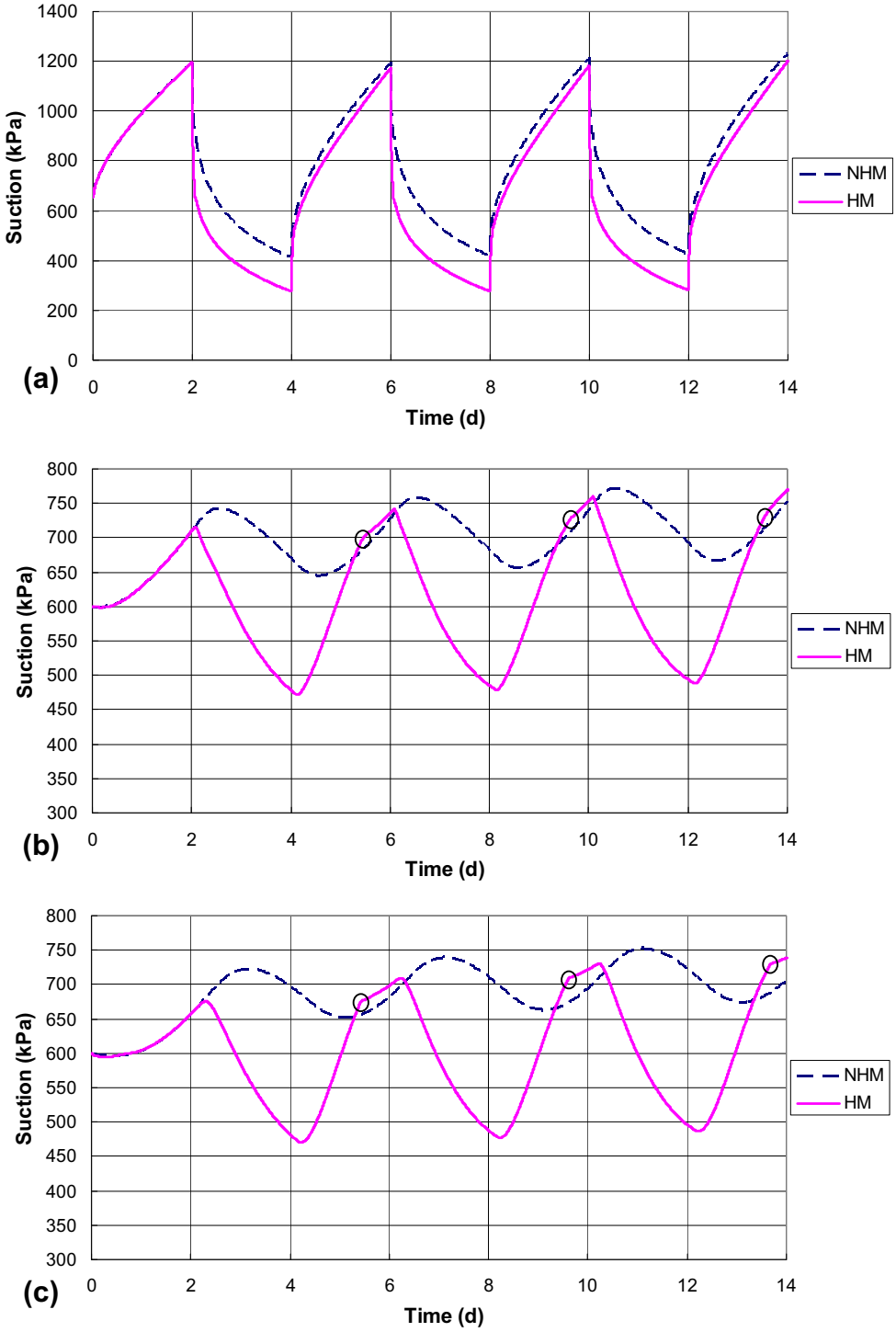

Fig. 6. Evolution of suction at different elevations of a one-layer soil column with time: (a) $y = 1.5$ m; (b) $y = 0.5$ m and (c) $y = 0.0$ m.

interface ($y = 0.3$ m), its hydraulic state always stays on the main wetting curve until the breakthrough occurs (Fig. 13c). After the breakthrough, the hydraulic state crosses the scanning zone and reaches the main drying curve. The soil at the lower side of the interface ($y = 0.25$ m) experiences a quick wetting upon the breakthrough (Fig. 13d). Due to the numerical method used, the accuracy of the numerical results is compromised by some observed oscillation. Therefore, further numerical elaboration should be undertaken to deal with the large contrast in the hydraulic properties on both sides of the interface of the two-layer soil column.

5.2. Case 2: Infiltration test on soil column of fine sand over medium sand [54]

Yang et al. [54] investigated the capillary effects by conducting infiltration tests on three soil columns of fine sand over medium sand (FM), medium sand over gravelly sand (MG), and fine sand over gravelly sand (FG). In this simulation, the experimental results for the FM column were employed to validate the hysteretic hydraulic model for unsaturated soils. The FM soil column had a thickness of 0.50 m for each layer, namely the upper fine sand

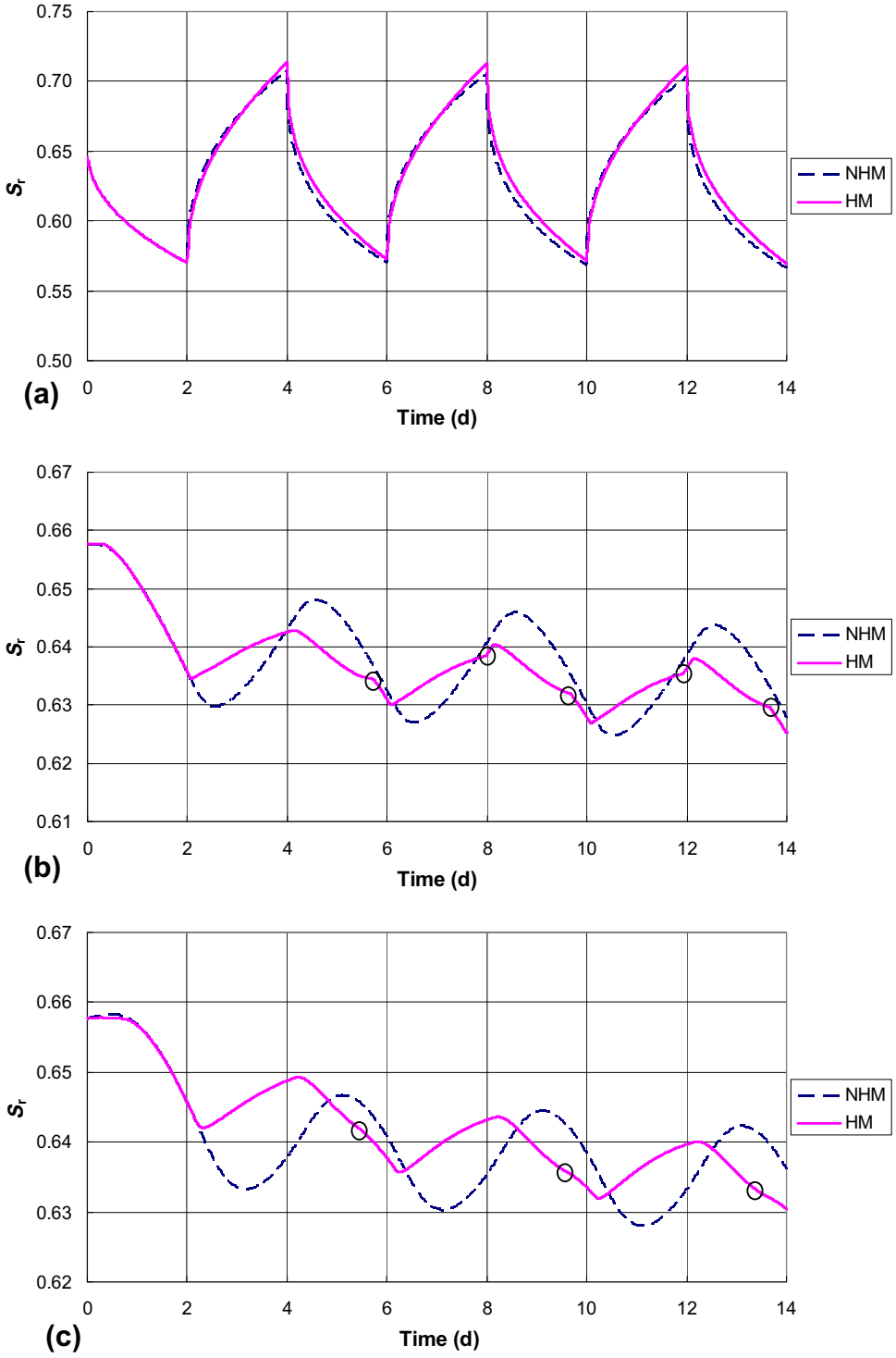

Fig. 7. Evolution of degree of saturation at different elevations of a one-layer soil column with time: (a) $y = 1.5$ m; (b) $y = 0.5$ m and (c) $y = 0.0$ m.

and the lower medium sand. Some basic parameters for the studied materials are presented in Table 3. Rainfall with an intensity of 1.10×10^{-5} m/s was applied at the top of the column for 1 h and then the test specimen was kept in a sealed environment for 63 days, while a constant water level remained at the bottom boundary (test FM-R2 in [54]). The initial state of the FM column was achieved by first an infiltration and then a redistribution process (test FM-R1). The detailed procedure for this experiment can be found in Yang et al. [54].

With the least square method, the soil water characteristic curve was calibrated by Zhang et al. [56] using the van Genuchten [48] equation according to the experimentally fitted Fredlund and Xing [16] parameters [54]. Zhang et al. [56] suggested that the main drying curve scaled from the main wetting curve should give better results for the observed data. Optimal values of the hysteretic ratio (ξ) for the fine and medium sands were reported as 1.86 and 2.85, respectively. The breakthrough head of the lower medium sand is 0.32 m when water from the upper layer starts to

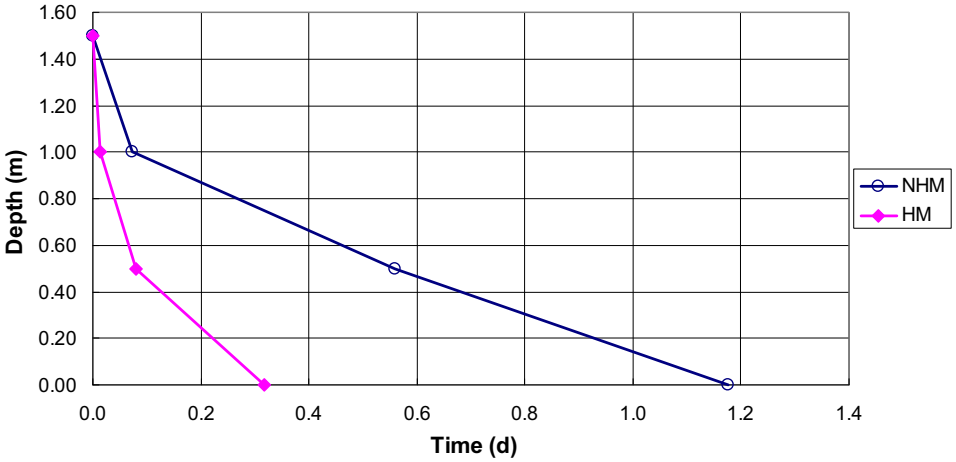

Fig. 8. Response delay in depth with respect to the 1st drying at the top surface of one-layer soil column.

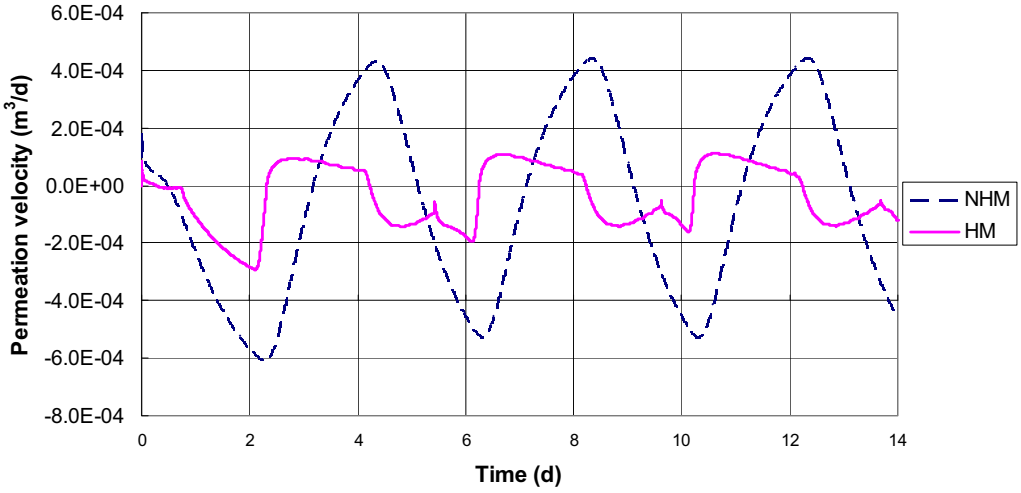

Fig. 9. Predicted flux velocity at the bottom of a one-layer soil column, $y = 0.0$ m.

Table 2
Hydraulic properties of silty sand and pea gravel.

	Symbol	Unit	Pea gravel	Silty sand
Saturated volumetric water content	θ_s	–	0.330	0.380
Residual volumetric water content	θ_r	–	0.030	0.070
Hydraulic conductivity				
Saturated hydraulic conductivity	k_s	m/d	1.123×10^{3}	2.592×10^{-1}
Parameters	c_k	–	1.000	1.000
	λ_k	–	4.000	2.500
Drying curve				
Restoration suction	ψ_d	kPa	0.800	–
Fitting parameters	α_d	kPa^{-1}	18.667	0.200
	n_d	–	2.5	2.020
Wetting curve				
Breakthrough suction	ψ_w	kPa	0.300	–
Fitting parameters	α_w	kPa^{-1}	28.000	0.300
	n_w	–	2.500	2.020
Scanning curve				
Scanning slope	κ_s	kPa^{-1}	6.29×10^{-3}	6.29×10^{-2}
	$r_{\kappa s}$	–	0.200	0.200

percolate into the lower layer. As suggested by Hillel [21], the restoration of a capillary barrier in soil covers may occur at about the same water content as the breakthrough. Thus the breakthrough and restoration suctions for the FM soil column can be deduced

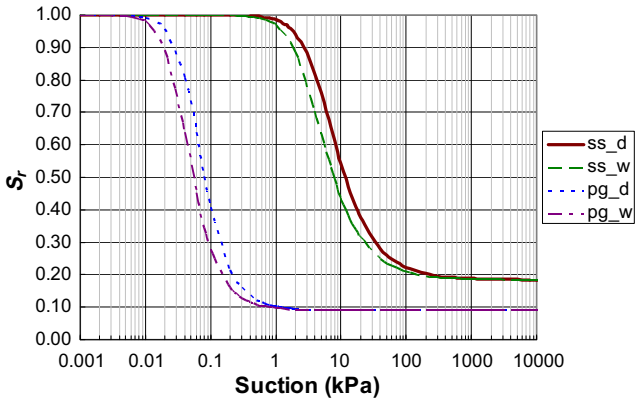

Fig. 10. SWCCs for soils used in the soil column infiltration test by Stormont and Anderson [46]. Silty sand is denoted as ss, and pea gravel as pg.

as 3.10 kPa and 8.00 kPa. Other parameters used in this analysis are listed in Table 3. The SWCCs for both the fine and medium sands are shown in Fig. 14. It is worth noting that the residual degree of saturation in the medium sand is even larger than that of the fine sand, which seems hard to explain depending solely on the information given by Yang et al. [54]. Nevertheless, in this paper, the original data are still used to fit the van Genuchten [48] equation.

The initial hydraulic condition directly determines the evolution of the hydraulic state in the unsaturated soil column. Therefore, in order to evaluate the capacity of the proposed hysteretic model, the most accurate description of the initial condition for test FM-R2 is necessary. Unfortunately, with only the suction profile provided at the end of test FM-R1 [54], it is difficult to describe accurately the initial condition. As a coarse estimation, the initial condition for test FM-R2 is assumed according to the results from the test FM-R1. Since in test FM-R1 the studied soil column experienced an initial intermittent infiltration and redistribution process of 20 days, wetting and drying mechanisms had been activated in the soil column with respect to the infiltration and moisture redistribution processes. Consequently, it is logical to assume proper hydraulic states for soils at different elevations as the initial condition for test FR-R2. In this modelling, the upper finer sand layer is approximately divided into three independent initial zones along the depth, namely, the main drying zone with elevation $y > 0.80$ m, the scanning zone with $0.7\ \text{m} \leqslant y \leqslant 0.8$ m, and the main wetting zone with $y < 0.70$ m. Further, to determine the initial scanning state within the main curves, an arithmetic average of the degrees of saturation on the main drying and wetting curves with respect to the same suction is adopted. A main wetting state is assumed throughout the lower medium sand layer, after consideration of the continuous downward movement of water from the upper layer in test FR-R1.

With the proposed hysteretic model, the numerical simulation of test FM-R2 was carried out and the results are presented Figs. 15–18. Fig. 15 shows the evolution with time of the hydraulic state at different elevations of the soil column in terms of suction and degree of saturation. Fairly good agreement can be observed between the numerical predictions and the experimental results. The hydraulic response of the soils studied is generally well captured by the hysteretic approach. For instance, during the first hour of infiltration, a significant amount of water enters the top layer, leading to a surge in the degree of saturation (Fig. 15b) and correspondingly a decrease in suction (Fig. 15a) in the near surface zone of the soil column. At the end of the rainfall ($t = 1$ h), the wetting front reaches an elevation of about 0.70 m (see Fig. 16). The infiltrated water continues to move downwards and finally at about $t = 3$ h it arrives at the interface between the upper and lower layers (see Fig. 15). Meanwhile, drying has started from the top of the soil column and gradually extends downwards as time elapses. This indicates that drying and wetting can coexist in the soil column, though at different elevations. In addition, the capillary barrier effect is able to be modelled by HM, as shown in Fig. 15. The water is temporarily held back at the capillary interface of the two-layer soil column ($y = 0.5$ m, Fig. 15b), inducing the suction decrease at the bottom of the upper finer sand layer (Fig. 15a). Meanwhile, consistent with the experimental data, almost no change occurs in the lower medium sand layer.

HM is capable of accurately describing the water breakthrough at the capillary interface in the soil column. Yang et al. [54] observed that the breakthrough starts in the period between 4 h and 6 h. As illustrated by Fig. 15, HM predicts the breakthrough at about $t = 4.93$ h, indicated by the abrupt drop in the suction value at the lower side of the capillary interface ($y = 0.45$ m). While water percolates into the medium sand, the suction gradually decreases and the medium sand becomes increasingly conductive, thereby progressively annulling the capillary barrier. With continuous drainage from the upper layer, the net flux at the upper side of the interface becomes negative. Thus the suction at the bottom of the fine sand layer ($y = 0.50$ m) starts to increase (Fig. 15a), indicating the initiation of a drying mechanism during this dynamic hydraulic state. Eventually if the restoration suction is reached, water will cease to move into the lower layer and the capillary barrier will be restored. But this restoration was not achieved in the experiment, and neither was it in the numerical prediction (Fig. 15).

The suction and water content profiles at different stages of test FM-R2 are depicted in Figs. 16 and 17. Comparisons with experimental data indicate that the proposed hysteretic model has the capability to predict the infiltration and redistribution in the soil column very well. The imposed water infiltrates into the soil column step by step, and wetting and drying occurs simultaneously at different elevations, which would be very difficult to model with conventional non-hysteretic models. Moreover, a significant decrease in suction and increase in the water content are observed between $t = 4$ h and $t = 6$ h at the capillary interface ($y = 0.50$ m), which corresponds to the occurrence of percolation of water into the lower layer and failure of the capillary barrier. Although the predicted water content cannot be corroborated by experimental data, this proposed model is believed to be able to offer more accurate results if the exact initial condition is known.

The hydraulic paths experienced by soils at different elevations of the soil column are shown in Fig. 18. At $y = 0.95$ m (Fig. 18a), the sand, which experiences drying initially (Point A) when subjected to the rainfall, moves along the scanning curve (A–B) towards the main wetting SWCC. When the hydraulic state reaches the main wetting curve (Point B), it continues to move along the main wetting curve (B–C) until the rainfall ceases ($t = 1$ h). Afterwards, the net outflow of water at $y = 0.95$ m is induced by the downward hydraulic gradient. Hence, drying at $y = 0.95$ m is reactivated, resulting in the hydraulic path back on the scanning curve (C–D), but this time towards the main drying SWCC. Fig. 18a illustrates that continuous drying in the moisture redistribution process causes the hydraulic state at $y = 0.95$ m to move along the main drying curve (D–E) until the final steady state (Point E) is obtained in the upper fine sand layer.

At $y = 0.75$ m (Fig. 18b), a similar hydraulic path to that at $y = 0.95$ m is observed. The only difference is that the initial hydraulic state lies in the scanning zone (Point A) at this elevation. Moreover, Fig. 18c and d shows similar hydraulic paths at $y = 0.50$ m and $y = 0.45$ m, even though the soils at these two elevations exhibit a huge contrast in their hydraulic properties. Drying at $y = 0.50$ m and wetting at $y = 0.45$ m are actually coupled during

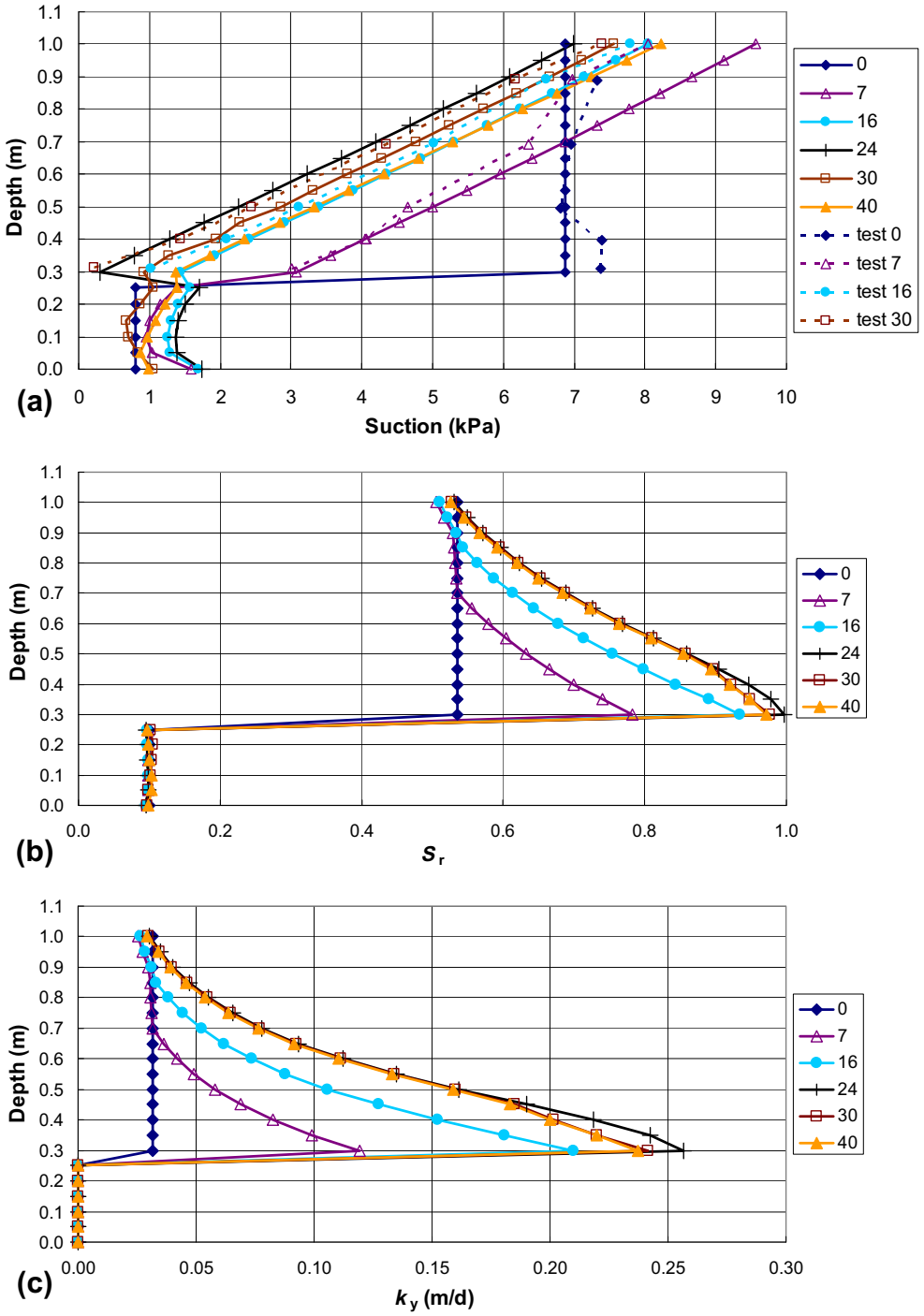

Fig. 11. Simulation of infiltration test on silty sand over pea gravel [46]: (a) suction profiles; (b) degree of saturation profiles and (c) hydraulic conductivity profiles.

breakthrough. When the breakthrough occurs, the soil at $y = 0.50$ m follows the drying scanning curve B–C in Fig. 18c, but the soil at 0.45 m follows the main wetting curve A–B in Fig. 18d. Therefore, with the hydraulic paths derived along the soil column, the hydraulic behaviour of the soil column can be understood more comprehensively.

5.3. Case 3: Infiltration test on soil column of fine over gravelly sand [22]

Indrawan et al. [22] conducted similar laboratory infiltration tests as Yang et al. [54] on a two-layer soil column. The two-layer soil column was packed with a 0.50 m thick upper finer layer overlying a 0.50 m thick lower coarser layer. The upper soil was a mixture of 50% reddish brown residual soil and 50% light grey to white gravelly sand, based on dry mass. The lower soil was a commercial gravelly sand. Experimental data on the soil water relationship of the two soils were fitted by the least-squares method to the van Genuchten [48] equation, as depicted in Fig. 19. It should be mentioned that in order to obtain closed hysteretic loops, the residual degree of saturation for the gravelly sand was not set purposely to zero. The reasonableness of this measure can also be inferred from Indrawan et al. [22]. The corresponding hydraulic parameters for the soil mixture and the gravelly sand are listed in Table 4. As

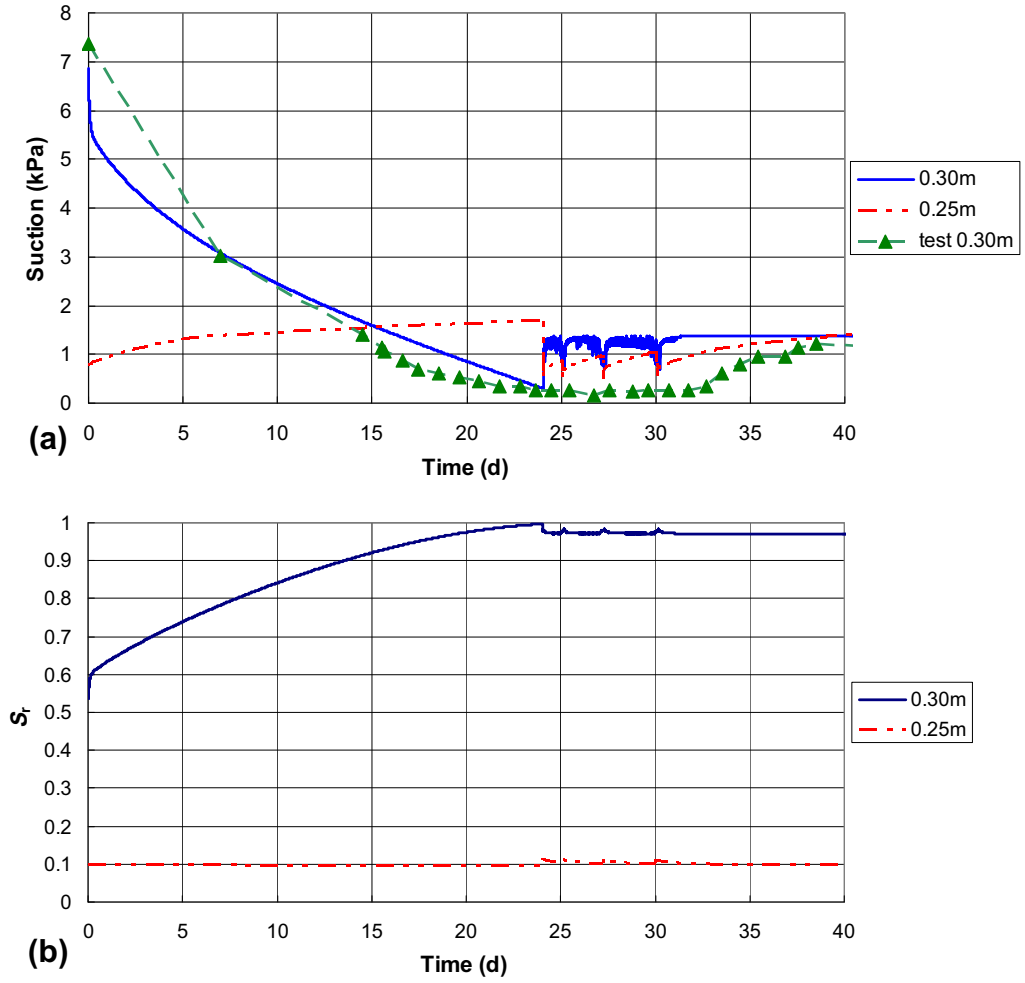

Fig. 12. Evolution of (a) suction and (b) degree of saturation in the infiltration test on silty sand over pea gravel column [46].

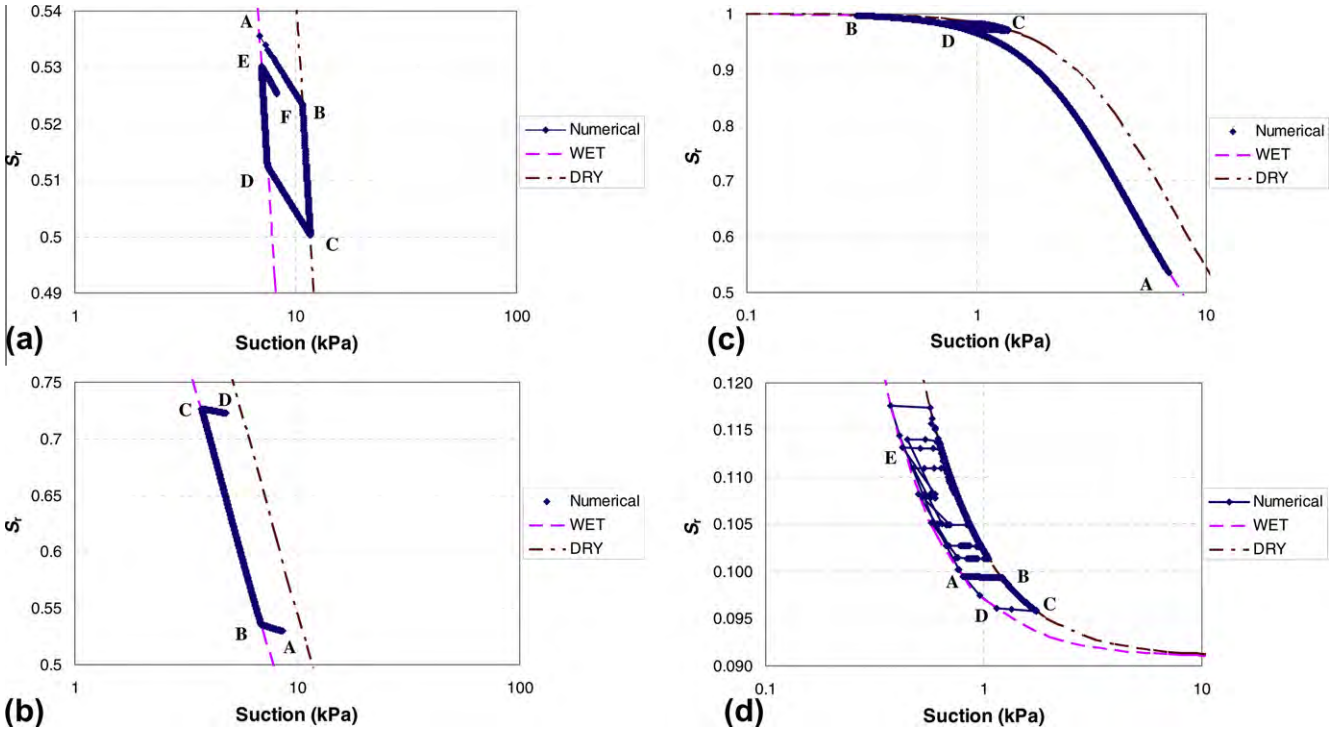

Fig. 13. Predicted hydraulic paths in the infiltration test on silty sand over pea gravel [46]: (a) y = 1.00 m; (b) y = 0.65 m, (c) y = 0.30 m and (d) y = 0.25 m.

Table 3
Hydraulic properties of fine sand and medium sand.

	Symbol	Unit	Medium sand	Fine sand
Saturated volumetric water content	θ_s	–	0.350	0.411
Residual volumetric water content	θ_r	–	6.260×10^{-2}	3.450×10^{-2}
Hydraulic conductivity				
Saturated hydraulic conductivity	k_s	m/h	0.720	0.972
Parameters	c_k	–	1.000	0.100
	λ_k	–	3.000	2.400
Drying curve				
Restoration suction	ψ_d	kPa	8.000	–
Fitting parameters	α_d	kPa^{-1}	0.720	0.403
	n_d	–	2.380	3.364
Wetting curve				
Breakthrough suction	ψ_w	kPa	3.100	–
Fitting parameters	α_w	kPa^{-1}	2.052	0.750
	n_w	–	2.380	3.364
Scanning curve				
Scanning slope	κ_s	kPa^{-1}	0.368	0.368
	$r_{\kappa s}$	–	0.200	0.200

suggested by Indrawan et al. [22], different values of λ_k in the hydraulic conductivity function (Eq. (2)) are used for the drying and wetting processes. In this paper, different values of λ_k at different hydraulic stages are further adopted to simulate the experimental results, as presented in Table 5.

Different types of infiltration tests were conducted by Indrawan et al. [22], including the upward infiltration test, a rapid drawndown test and a rainfall test. The upward infiltration test was first carried out to saturate the soil column and to derive the saturated hydraulic conductivity of each layer. The rapid drawdown test was then conducted to obtain a static equilibrium condition in the soil mixture layer and a static non-equilibrium condition in the gravelly sand layer. A rainfall test was finally activated on the top of the soil column for a certain duration and then the soil column was left for enough time to permit the moisture redistribution process.

Indrawan et al. [22] also carried out numerical modelling of the experimental soil column, and suggested that the main wetting curve should be used in the simulation of the wetting process while the main drying curve was appropriate for the drying process. Such an approach artificially split the rainfall and the subsequent moisture redistribution phases into two independent processes for the soil column, which implies that the whole soil column undergoes wetting and drying separately. In reality, as concluded in Case 1 presented previously, some drying may even occur in the soil during the rainfall phase, and some wetting is also possible during the moisture redistribution, particularly in the lower suction zone of the soil column, as evidenced in Case 2. Thus, drying and wetting mechanisms may coexist in the same soil column as moisture redistribution occurs. In this paper, the hysteretic model has been used to simulate the infiltration test conducted by Indrawan et al. [22].

Simulation of the final rainfall and redistribution process is presented in Figs. 20–24. The final state of the previous drawdown test was used as the initial condition for the rainfall tests. According to the static equilibrium condition observed in the experiment, a linear hydraulic head profile with a slope value of -1 was adopted as the initial condition for the upper soil mixture. The upper layer was assumed to lie initially on the main drying curve, except for soil at the elevation $y = 0.85$ m, which was assumed to be on the main wetting curve considering its unusually low initial volumetric water content, as reported by Indrawan et al. [22]. For the lower gravelly sand, a fitted hydraulic head with respect to the experimental data was

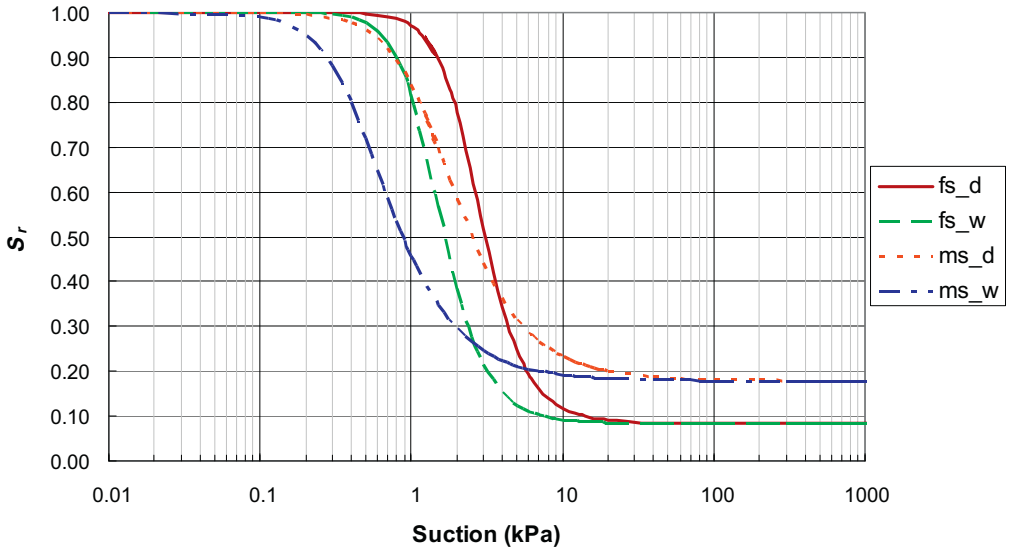

Fig. 14. SWCCs for soils used in the soil column infiltration test by Yang et al. [54]. *Note*: Fine sand is abbreviated as fs, and medium sand as ms.

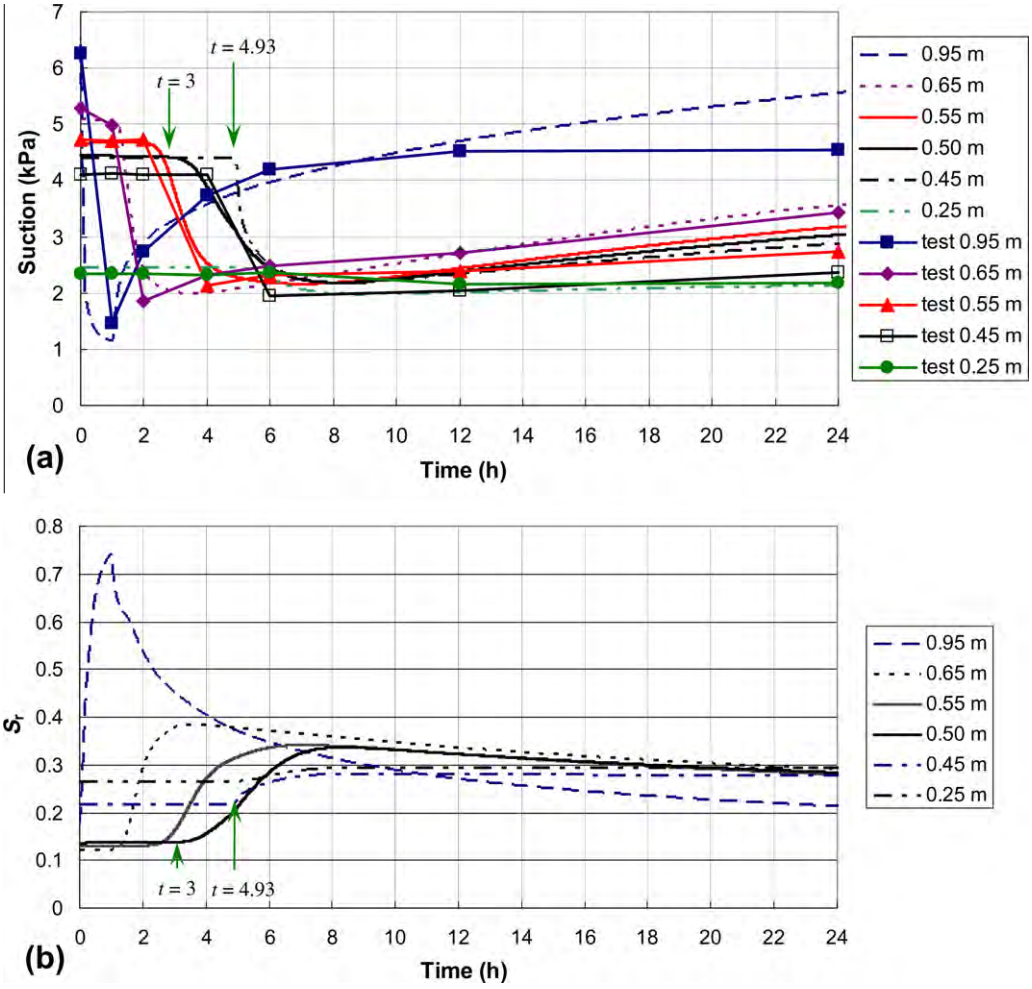

Fig. 15. Evolution of (a) suction and (b) degree of saturation with time in the infiltration test on the soil column of fine sand over medium sand (FM-R2 from Yang et al. [54]).

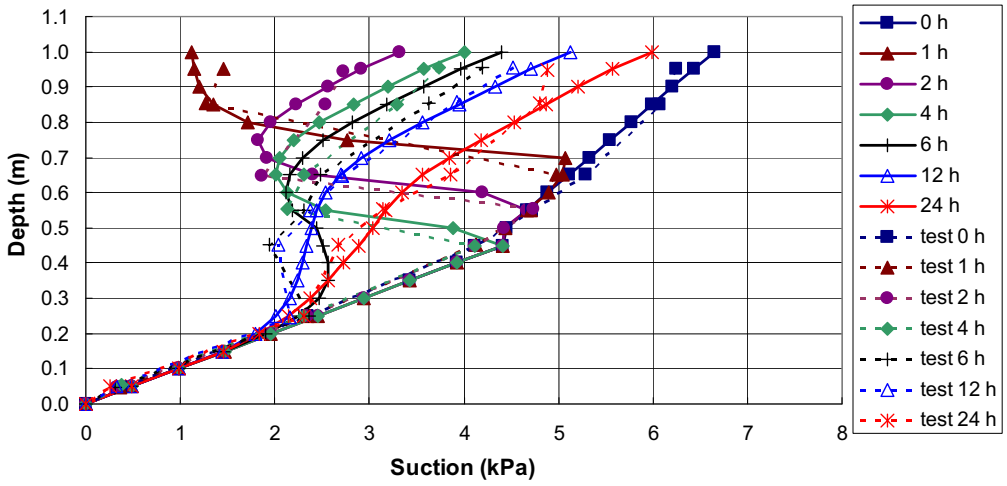

Fig. 16. Suction profiles in the infiltration test on the soil column of fine sand over medium sand (FM-R2 from Yang et al. [54]).

used as the initial condition and the whole layer was assumed to be on the main drying curve. To simulate the static non-equilibrium condition of the gravelly sand, an extremely low hydraulic conductivity was maintained by a proper choice of λ_k values.

In accordance with the experimental procedure, the boundary condition at the bottom of the soil column was set to a constant water table (h = 0 m) throughout the rainfall test. As for the boundary condition on the top of soil column, a rainfall with an intensity of 9 mm/h and 2 h duration was imposed and then zero-flux was maintained throughout the rest of the test. Evaporation was avoided by placing an acrylic plate cover on the top of the soil column.

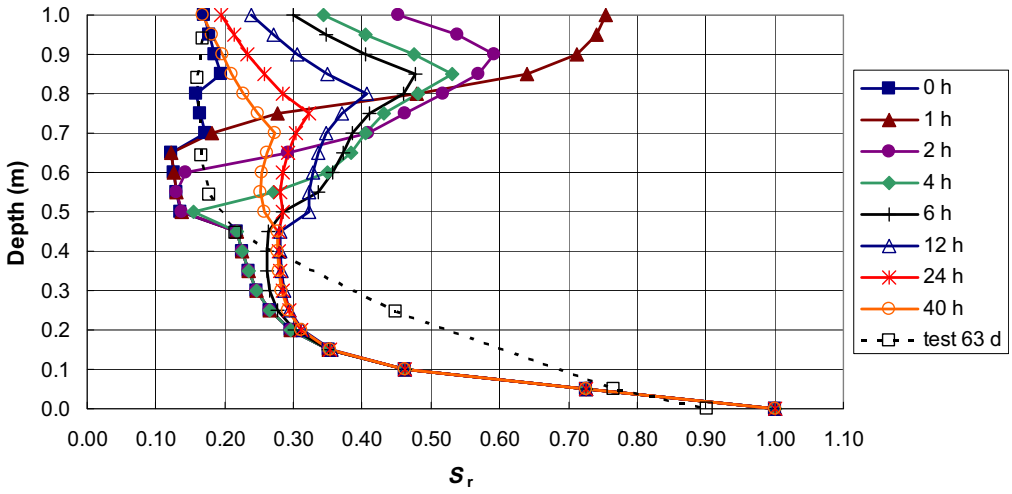

Fig. 17. Degree of saturation profiles in the infiltration test on the soil column of fine sand over medium sand (FM-R2 from Yang et al. [54]).

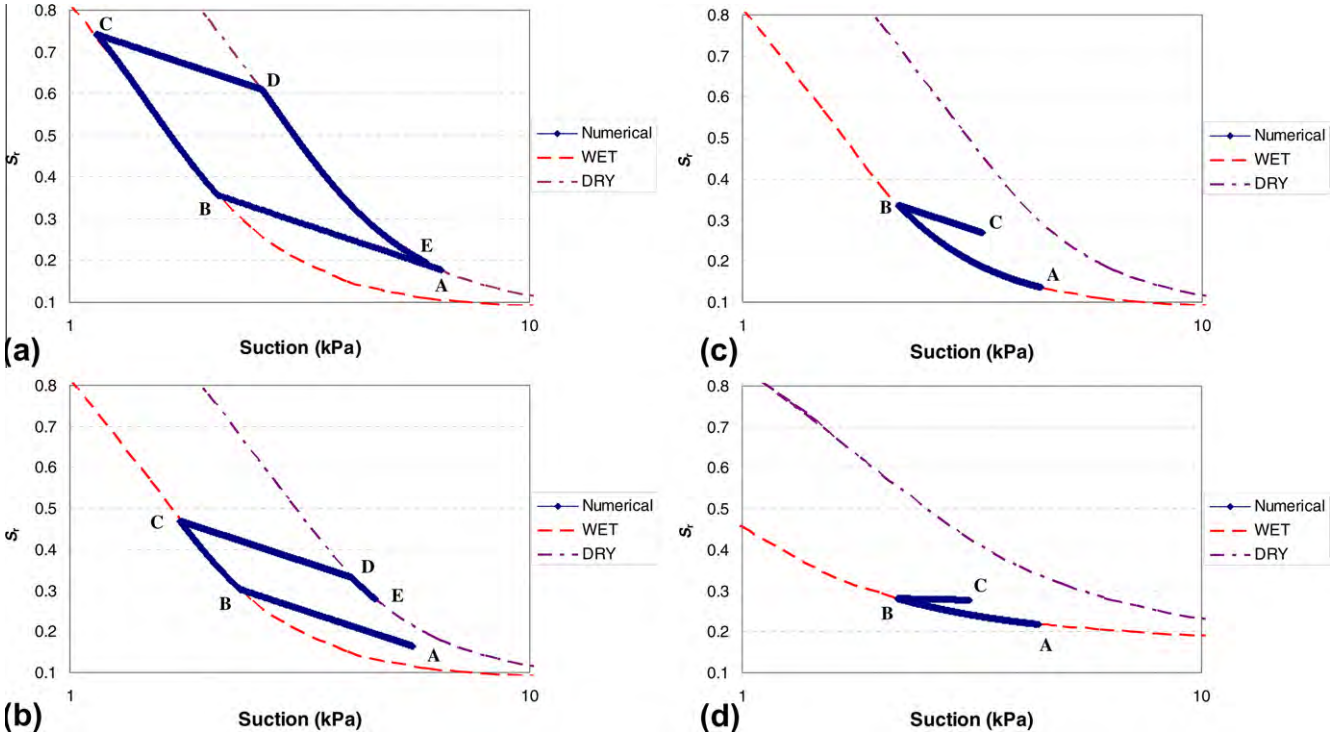

Fig. 18. Hydraulic paths in the infiltration test on the soil column of fine sand over medium sand (FM-R2 from Yang et al. [54]): (a) $y = 0.90$ m, (b) $y = 0.75$ m, (c) $y = 0.50$ m, and (d) $y = 0.45$ m.

Fig. 20 shows a comparison between the suction profiles obtained from the hysteretic model and the laboratory experiments. Good agreement between the two is achieved. In the rainfall phase, from $t = 0$ h to $t = 2$ h (Fig. 20a), water infiltrated into the soil column from the top and flowed gradually downward, thereby leading to a gradual decrease in suction with depth. The breakthrough at the fine-over-coarse interface is predicted to happen between $t = 1$ h and $t = 2$ h (Fig. 20a), slightly earlier than the experimental observation which is in the period between $t = 2$ h and $t = 3$ h. The decrease of suction in the gravelly sand after the water percolation is also captured by the model.

When the rainfall stopped at $t = 2$ h, the suction profiles of the soil column developed as shown in Fig. 20b. In the soil mixture layer, drying was induced in the region defined by $y > 0.60$ m due to the net downward flux of water. Meanwhile, wetting continued in the zone defined by $0.60 \geqslant y \geqslant 0.50$ m, as water still infiltrated from above. As time elapsed, the soil mixture layer approached the static equilibrium state gradually. In the lower gravelly sand layer, drying started as soon as the percolation stopped. As the percolated water flowed out, suction increased uniformly throughout the lower layer, but only to a small extent. The static non-equilibrium state was maintained finally, due to the extremely low hydraulic conductivity in the gravelly sand.

Fig. 21 shows the degree of saturation profiles of the soil column during the infiltration test. It can be seen that, corresponding to the suction profiles (Fig. 20), the degree of saturation increased

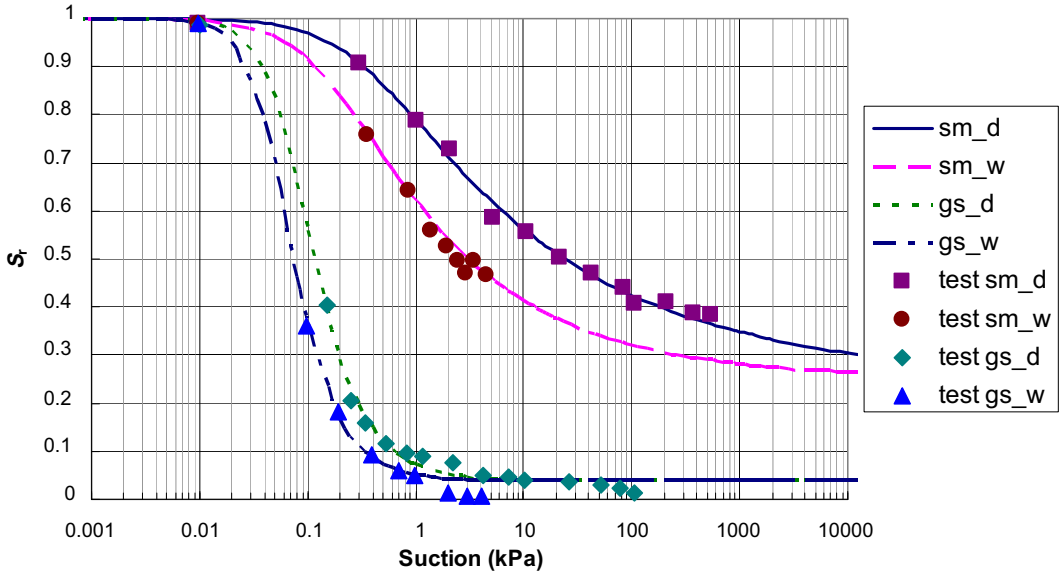

Fig. 19. SWCCs for soils used in the soil column infiltration test by Indrawan et al. [22]. *Note*: Soil mixture is abbreviated as sm, and gravelly sand as gs.

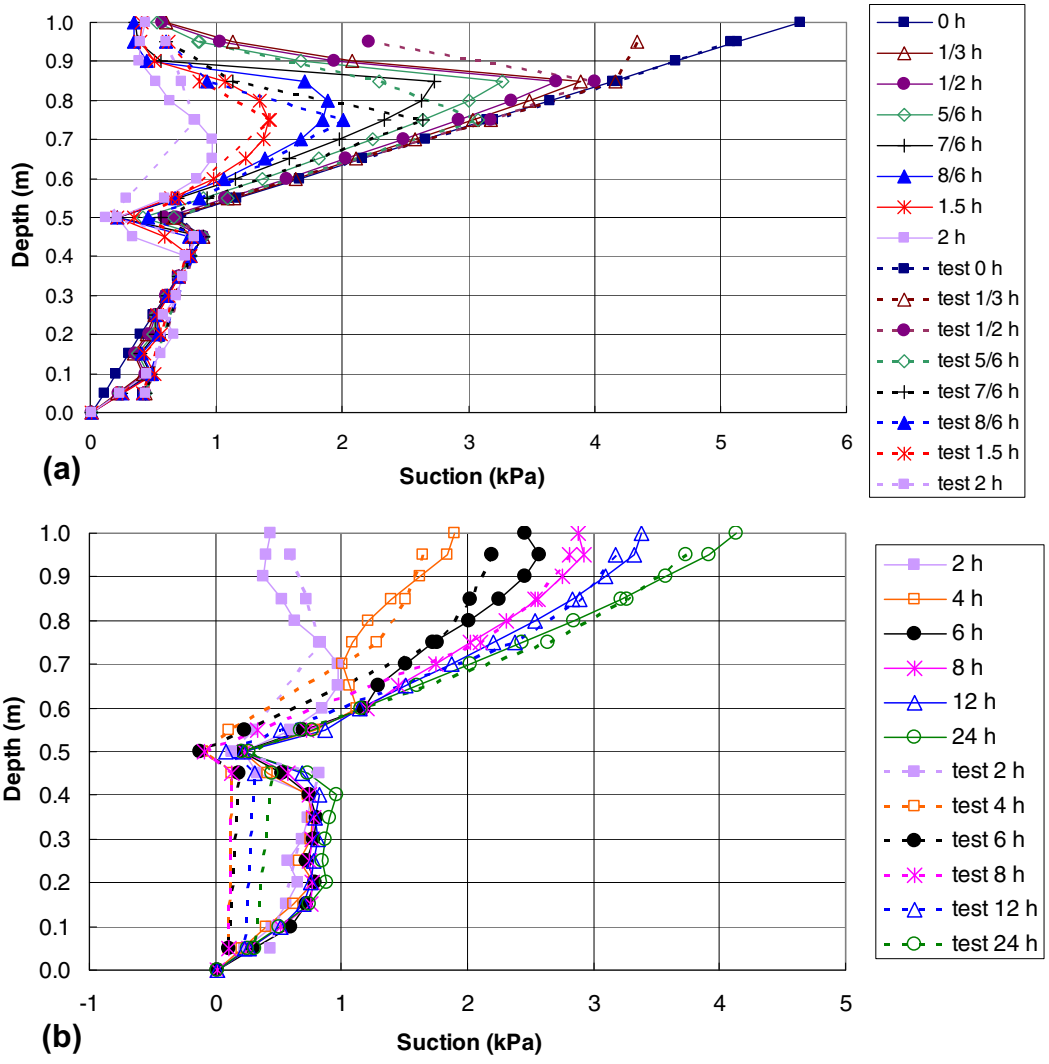

Fig. 20. Suction profiles in the infiltration test on the soil column of soil mixture over gravelly sand [22]: (a) $t \leqslant 2$ h and (b) $t \geqslant 2$ h.

Table 4
Hydraulic properties of soil mixture and gravelly sand.

	Symbol	Unit	Gravelly sand	Soil mixture
Saturated volumetric water content	θ_s	–	0.382	0.339
Residual volumetric water content	θ_r	–	1.470×10^{-2}	8.530×10^{-2}
Hydraulic conductivity				
Saturated hydraulic conductivity	k_s	m/h	2.736×10^{2}	7.560×10^{-1}
Correction coefficient for $k(\theta)$	c_k	–	1.000	0.100
Drying curve				
Restoration suction	ψ_d	kPa	0.250	–
Fitting parameters	α_d	kPa^{-1}	13.481	3.078
	n_d	–	2.286	1.256
Wetting curve				
Breakthrough suction	ψ_w	kPa	0.205	3.061
Fitting parameters	α_w	kPa^{-1}	19.396	6.627
	n_w	–	2.469	1.366
Scanning curve				
Scanning slope	κ_s	kPa^{-1}	0.023	0.035
	$r_{\kappa s}$	–	0.200	0.200

Table 5
Optimization of λ_k values according to the infiltration results.

Period (h)	SWCC	Gravelly sand	Soil mixture
$t \leqslant 1$	Drying	6.00	6.00
	Wetting	4.90	5.00
$t \leqslant 2$	Drying	6.00	6.00
	Wetting	4.90	5.00
$t > 2$	Drying	13.00	6.40
	Wetting	6.80	5.10

in the upper part of the soil mixture when the rainfall proceeded and decreased when the rainfall stoped. The predicted degrees of saturation generally agree with the experimental data throughout the soil column, except at $y = 0.85$ m. As reported by Indrawan et al. [22], the unusually low volumetric water content at $y = 0.85$ m was most likely caused by error in the TDR reading at this elevation. If verification of the TDR measurement by the oven drying method is considered (Fig. 22), the predicted degree of saturation is fairly reasonable at $y = 0.85$ m. However, limited by the available data from the oven drying method, data obtained by the TDR were used to validate the proposed hysteretic model.

To illustrate further the capacity of the proposed hysteretic model, the evolution with time of both suction and the degree of saturation are compared with experimental results, as depicted in Fig. 23. In general, the proposed model predicts well the hydraulic behaviour of the soil column. The predictions could be further improved if more accurate descriptions of the initial condition and the hydraulic properties of the soil column were available.

The hydraulic paths experienced by soils at different elevations in the soil column are illustrated in Fig. 24. Regardless of the initial

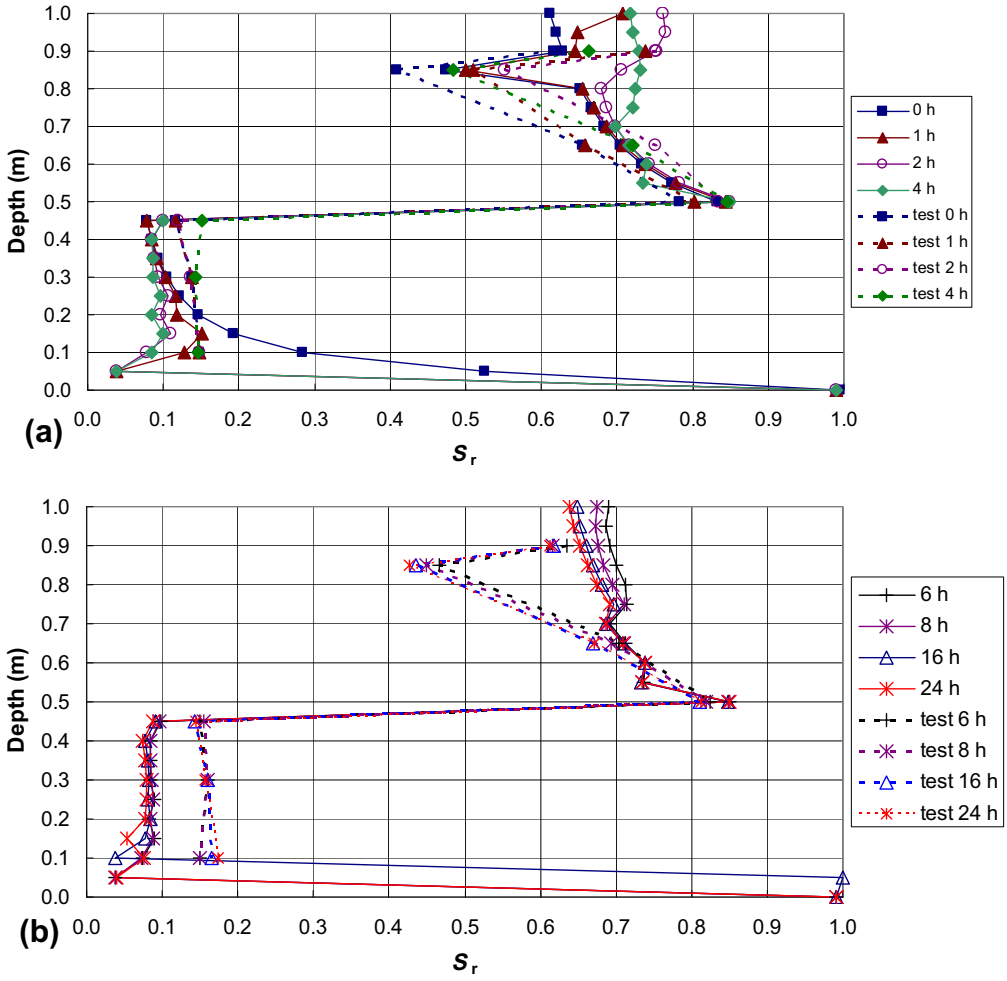

Fig. 21. Degree of saturation profiles in the infiltration test on the soil column of soil mixture over gravelly sand [22]: (a) $t \leqslant 4$ h and $t \geqslant 6$ h.

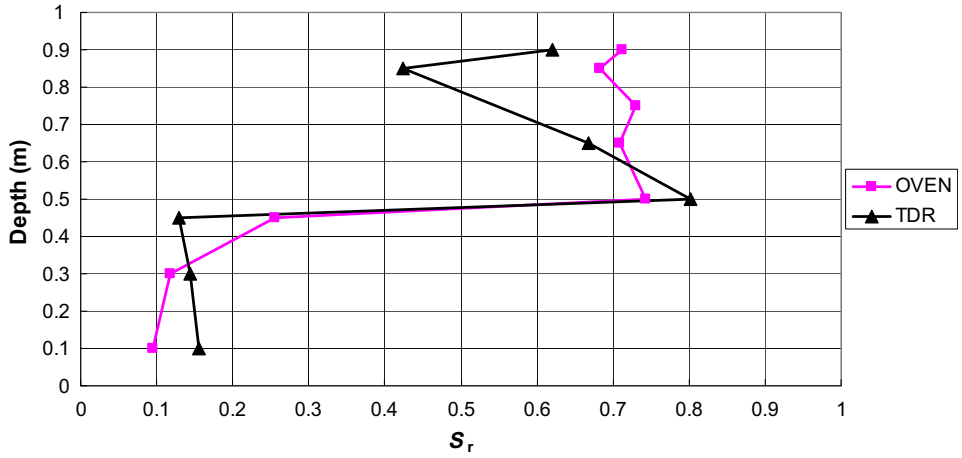

Fig. 22. Calibration of water content measured by TDR with oven drying method (redrawn from Indrawan et al. [22]).

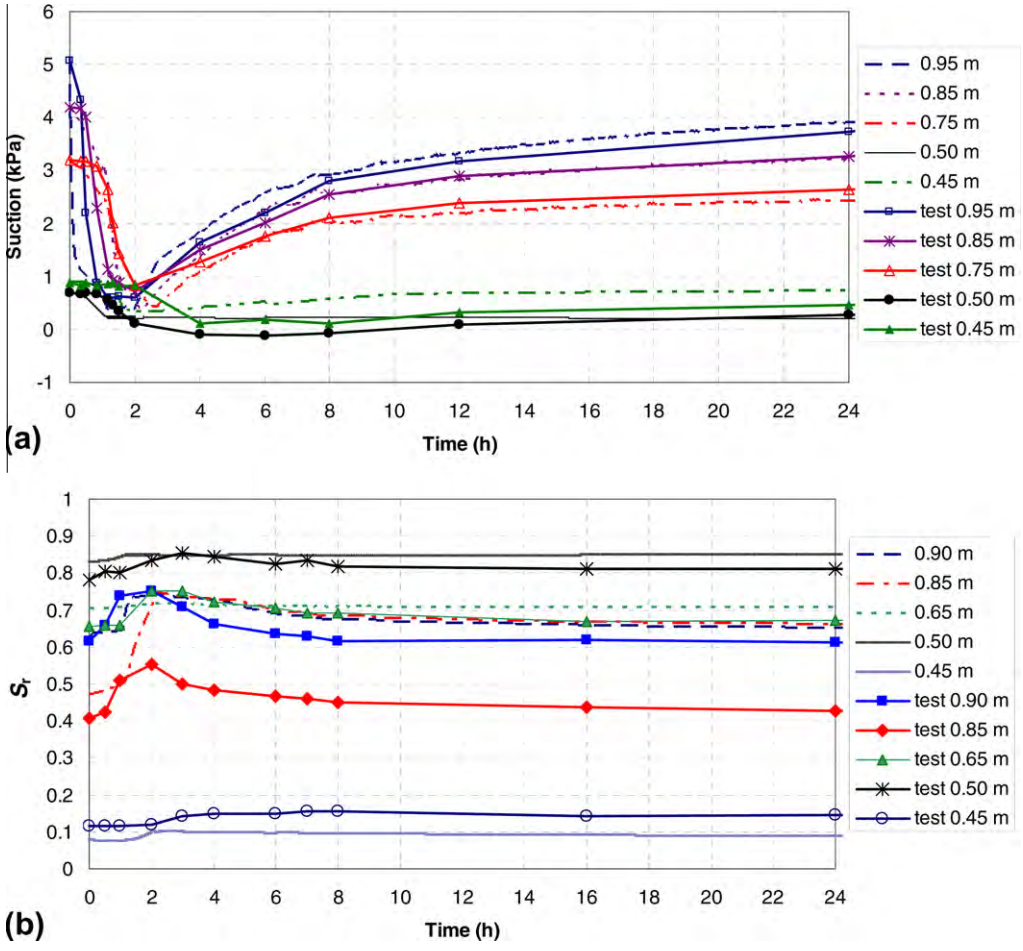

Fig. 23. Evolution of (a) suction and (b) water content at different elevations of soil column during the rainfall test.

states, soils throughout the soil column experience a first wetting and a subsequent drying process. It is worth noting that a hysteretic loop is clearly observed at the elevations given by $y = 0.85$ and $y = 0.45$ m in the experimental data (Fig. 24c and d), though some discrepancies exist among the experimental data themselves. Again, the hysteretic model is capable of capturing this phenomenon properly.

The numerical analyses described here indicate that drying and wetting, as two different hydraulic processes, can generally coexist in the same soil column, which necessitates the use of the hysteretic model in analysing soil covers. However, these three cases have not allowed the full advantages of the hysteretic model over the non-hysteretic model to be demonstrated, due to the tested soil samples displaying relatively minor hysteresis. Nevertheless, the essential differences between the two models, HM and NHM, have been clearly demonstrated.

It is planned to conduct seepage experiments in compacted clay columns in the future to deepen the understanding of the hysteretic

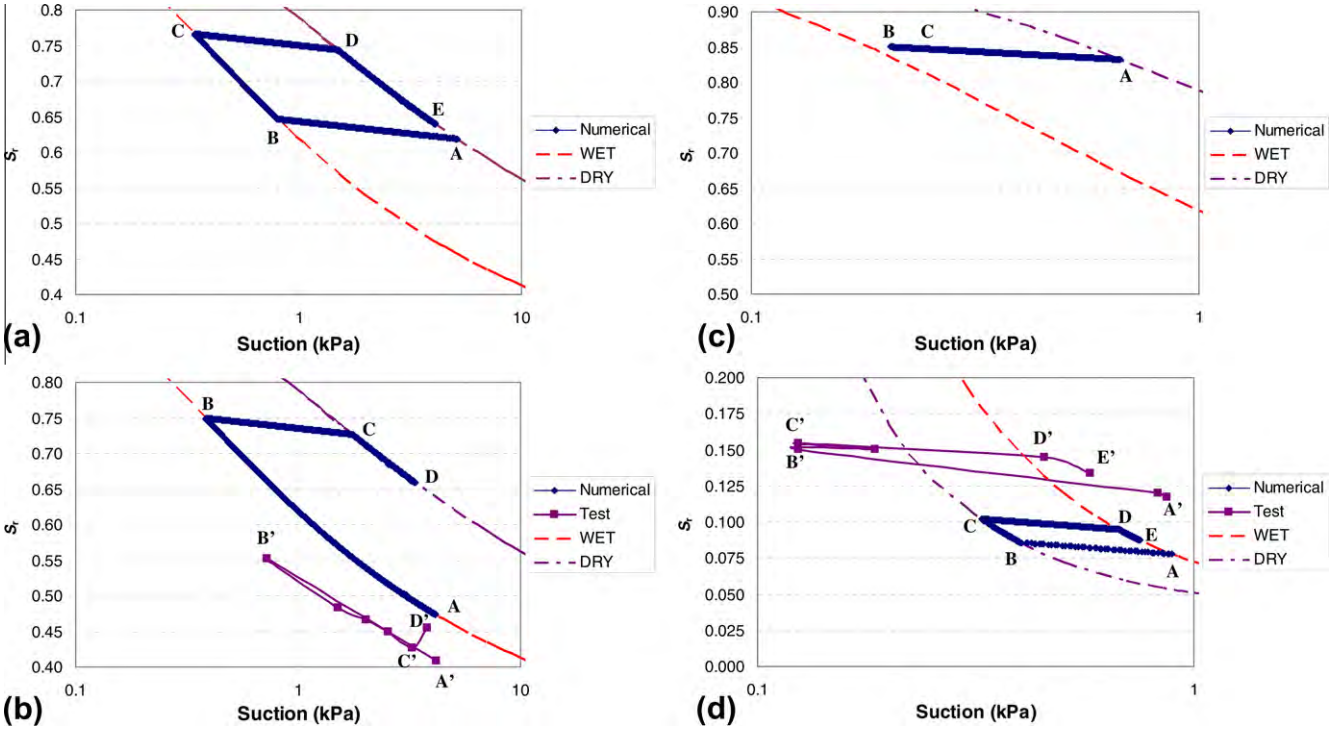

Fig. 24. Hydraulic paths at different elevations of the soil column during the infiltration test: (a) $y = 0.95$ m, (b) $y = 0.85$ m, (c) $y = 0.50$ m and (d) $y = 0.45$ m.

effects. The hysteretic model itself requires further elaboration in at least two important aspects: a more accurate description of the basic hydraulic behaviour and the numerical implementation techniques adopted to solve the governing equation. Convergence and oscillation problems at the fine-over-coarse interface were again encountered in Case 3, as indicated in Fig. 23a. In addition, the importance of a proper description of the initial conditions should also be highlighted in numerical seepage analysis. This factor is equally important for both hysteretic and non-hysteretic models.

6. Conclusions

The effects of hydraulic hysteresis on the hydraulic behaviour of unsaturated soils have been investigated. The hysteretic soil water characteristic curve and hydraulic conductivity were incorporated into the *h*-based Richards equation to analyse transient seepage in unsaturated soils subjected to cyclic drying and wetting. The finite difference method was used to solve the seepage problem under various boundary conditions. Predictions of the hysteretic model (HM) were compared with those of the traditional non-hysteretic model (NHM) for a one-dimensional compacted clay column subjected to cyclic drying and wetting. It was found that compared with the NHM, the HM leads to a wider range of variation in suction and a relatively larger average percolation velocity in the soil column, especially in soils with significant hysteresis. This difference highlights that caution should be exercised when the non-hysteretic model is applied to analyse the hydraulic performance of engineered soil covers, especially of those composed of highly hysteretic materials.

Further predictions of the hysteretic model were compared against laboratory experiments. Three infiltration tests on one-dimensional capillary columns were employed as benchmark data. The mechanism of capillary tension was incorporated in the hysteretic model to simulate the capillary barrier effect in two-layer soil columns. Both the experiments and numerical simulations demonstrate that drying and wetting can simultaneously occur in different parts of the soil, which further motivates an integrated treatment of hydraulic hysteresis in seepage analysis. The hysteretic model was generally successful in reproducing the experimental data. In addition, the HM can clearly predict the hydraulic state in the soil column, which is important for the performance evaluation of soil covers.

Some further work is required to elaborate the model. The description of hydraulic conductivity of unsaturated soils adopted in this paper is still relatively crude, and could be replaced by more accurate models. Numerical convergence and stability problems still exist in the hysteretic model when using the finite difference method to solve the governing equations, which calls for more advanced numerical techniques for solving these highly non-linear partial differential equations. More seepage experiments in soil covers displaying more pronounced hydraulic hysteresis, e.g., compacted clay, should be conducted to further test the applicability and efficiency of the proposed hysteretic model.

References

[1] Adu-wusu C, Yanful EK, Lanteigne L, O'Kane M. Prediction of the water balance of two soil cover systems. Geotech Geol Eng 2007;25:215–37.
[2] Averjanov SF. About permeability of subsurface soils in case of incomplete saturation. The theory of ground water movement; 1950. p. 19–21.
[3] Benson CH, Daniel DE, Boutwell GP. Field performance of compacted clay liners. J Geotech Geoenviron Eng 1999;125(5):390–403.
[4] Brooks RH, Corey AT. Hydraulic properties of porous media. Colorado State University Hydrology Paper, Fort Collins, Nr. 3; 1964. p. 27.
[5] Bussiere B, Aubertin M, Chapuis RP. The behaviour of inclined covers used as oxygen barriers. Can Geotech J 2003;40:512–35.
[6] Bussiere B, Aubertin M, Mbonimpa M, Molson JM, Chapuis RP. Field experimental cells to evaluate the hydrogeological behaviour of oxygen barriers made of silty materials. Can Geotech J 2007;44:245–65.
[7] Campbell JD. Pore pressures and volume changes in unsaturated soils. PhD thesis, University of Illinois at Urbana-Champaign, Urbana-Champaign, IL; 1973.
[8] Celia MA, Boulouta ET, Zarba R. A general mass-conservative numerical solution for the unsaturated flow equation. Water Resour Res 1990;26(7):1483–96.
[9] Childs EC, Collis-George GN. The permeability of porous materials. Proc Roy Soc Lond Ser A 1950;201:392–405.

[10] Chiu TF, Shackelford CD. Unsaturated hydraulic conductivity of compacted sand–kaolin mixtures. J Geotech Geoenviron Eng 1998;124(2):160–70.
[11] Croney D, Coleman JD. Pore pressure and suction in soils. In: Proceeding of pore pressure and suction in soils, Butterworths, London; 1961. p. 31–7.
[12] Dane JH, Wierenga PJ. Effect of hysteresis on the prediction of infiltration, redistribution and drainage of water in a layered soil. J Hydrol 1975;25:229–42.
[13] Dye HB, Houston SL, Welfert BD. Influence of unsaturated soil properties uncertainty on moisture flow modelling. J Geotech Geol Eng 2009.
[14] Fala O, Molson J, Aubertin M, Bussiere B. Numerical modelling of flow and capillary barrier effects in unsaturated waste rock piles. Mine Water Environ 2005;24:172–85.
[15] Fredlund DG, Rahadjo H. Soil mechanics for unsaturated soils. New York: John Wiley and Sons, Inc.; 1993.
[16] Fredlund DG, Xing A. Equations for the soil–water characteristic curve. Can Geotech J 1994;31:521–32.
[17] Fredlund DG, Xing A, Huang S. Predicting the permeability function for unsaturated soils using the soil–water characteristic curve. Can Geotech J 1994;31:533–46.
[18] Garder WR. Some steady state solutions of the unsaturated moisture flow equation with application to evaporation from a water table. Soil Sci 1958;85:228–32.
[19] Haines WB. Studies in the physical properties of soil: V. The hysteresis effect in capillary properties, and the modes of moisture associated therewith. J Agric Sci 1930;20:97–116.
[20] Hanks RJ, Klute A, Bresler E. A numeric model for estimating infiltration, distribution, drainage and evaporation of water from soil. Water Resour Res 1969;5:1064–9.
[21] Hillel D. Introduction to soil physics. San Diego: Academic; 1980.
[22] Indrawan IGB, Rahadjo H, Leong EC. Drying and wetting characteristics of a two-layer soil column. Can Geotech J 2007;44:20–32.
[23] Jaynes DB. Comparison of soil–water hysteresis models. J Hydrol 1984;75:287–99.
[24] Khire MV, Benson CH, Bosscher PJ. Capillary barriers: design variables and water balance. J Geotech Geoenviron Eng 2000;126:695–708.
[25] Kool JB, Parker JC. Development and evaluation of closed-form expressions for hysteretic hydraulic properties. Water Resour Res 1987;23(1):105–14.
[26] Leong EC, Rahardjo H. Permeability functions for unsaturated soils. J Geotech Geoenviron Eng 1997;123(12):1118–26.
[27] Li XS. Modelling of hysteresis response for arbitrary wetting/drying paths. Comput Geotech 2005;32:133–7.
[28] Luckner L, van Genuchten MTh, Nielsen DR. A consistent set of parametric models for the two-phase flow of immiscible fluids in the subsurface. Water Resour Res 1989;25(10):2187–93.
[29] Malusis MA, Shackelford CD. Chemico-osmotic efficiency of a geosynthetic clay liner. J Geotech Geoenviron Eng 2002;128(2):97–106.
[30] Malusis MA, Shackelford CD, Olsen HW. Flow and transport through clay membrane barriers. Eng Geol 2003;70:235–48.
[31] Meerdink J, Benson C, Khire M. Unsaturated hydraulic conductivity of two compacted barrier soils. J Geotech Eng 1996;122(7):565–76.
[32] Melchior S. In-situ studies on the performance of landfill caps compacted soil liners, geomembranes, geosynthetic clay liners, capillary barriers. In: Proc 1997 international containment technology conference, St. Petersburg, Florida, USA, February 9–12, 1997. p. 365–73.
[33] Molson JW, Aubertin M, Joanes AM, Bussière B. Simulating acid mine drainage through mine wastes constructed with capillary barrier covers. In: Proceedings of the 5th joint IAH-CNC and CGS groundwater specialty conference, 57th Canadian geotechnical conference, Québec City, Que., 24–27 October 2004. Canadian Geotechnical Society, Richmond, B.C. Session 8D. p. 29–36.
[34] Morris CE, Stormont JC. Capillary barriers and subtitle D covers: estimating equivalency. J Environ Eng 1997;123(1):3–10.
[35] Mualem Y. Hysteretical models for prediction of the hydraulic conductivity of unsaturated porous media. Water Resour Res 1976;12:1248–54.
[36] Mualem Y, Miller EE. A hysteresis model based on an explicit domain-dependence function. Soil Sci Soc Am J 1979;43:1067–73.
[37] O'Kane M, Wilson GW, Barbour SL. Instrumentation and monitoring of an engineered soil cover system for mine waste rock. Can Geotech J 1998;35:828–46.
[38] Oldenburg CM, Pruess K. On numerical modelling of capillary barriers. Water Resour Res 1993;29(4):1045–56.
[39] Richards LA. Capillary conduction of liquids through porous mediums. Physics 1931;1:318–33.
[40] Romero E, Gens A, Lloret A. Water permeability, water retention and microstructure of unsaturated compacted Boom clay. Eng Geol 1999;54:117–27.
[41] Ross B. The diversion capacity of capillary barriers. Water Resour Res 1990;26(10):2625–9.
[42] Sheng D, Fredlund DG, Gens A. A new modelling approach for unsaturated soils using independent stress variables. Can Geotech J 2008;45(4):511–34.
[43] Sheng D, Gens A, Fredlund DG, Sloan SW. Unsaturated soils: from constitutive modelling to numerical algorithms. Comput Geotech 2008;35:810–24.
[44] Simms PH, Yanful EK. Some insights into the performance of an experimental soil cover near London, Ontario. Can Geotech J 1999;36:846–60.
[45] Stormont JC. Performance of two capillary barriers during constant infiltration. Geotech Spec Publ, ASCE 1995;53:77–92.
[46] Stormont JC, Anderson CE. Capillary barrier effect from underlying coarser soil layer. J Geotech Geoenviron Eng 1999;125(8):641–8.
[47] Tami D, Rahardjo H, Leong EC. Effects of hysteresis on steady-state infiltration in unsaturated slopes. J Geotech Geoenviron Eng 2004;130(9):956–66.
[48] van Genuchten MTh. A closed-form equation for predicting the hydraulic conductivity of unsaturated soils. Soil Sci Soc Am J 1980;44:892–8.
[49] van Genuchten MTh, Nielsen DR. On describing and predicting the hydraulic properties of unsaturated soils. Ann Geophys 1985;3(5):615–28.
[50] Vogel T, van Genuchten MTh, Cislerova M. Effect of the shape of the soil hydraulic functions near saturation on variably-saturated low predictions. Adv Water Resour 2000;24:133–44.
[51] Yanful EK, Mousavi SM, De Souza L. A numerical study of soil cover performance. J Environ Manage 2006;81:72–92.
[52] Yanful EK, Riley MD, Duncan J. Construction and monitoring of a composite soil cover on an experimental waste-rock pile near Newcastle, New Brunswick, Canada. Can Geotech J 1993;30:588–99.
[53] Yanful EK, Simms PH, Payant SC. Soil covers for controlling acid generation in mine tailings: a laboratory evaluation of the physics and geochemistry. Water, Air, and Soil Pollut 1999;114:347–75.
[54] Yang H, Rahardjo H, Leong EC, Fredlund DG. A study of infiltration on three sand capillary barriers. Can Geotech J 2004;41(4):629–43.
[55] Yang C, Sheng D, Carter JP. Numerical modelling of hydraulic hysteresis in unsaturated soil covers. In: 13th International conference of the IACMAG 2011, Melbourne, Australia; 2011. p. 741–6.
[56] Zhang Q, Werner AD, Aviyanto RF, Hutson JL. Influence of soil moisture hysteresis on the functioning of capillary barriers. Hydrol Process 2009;23(9):1369–75.